Electron small polarons and bipolarons in $LiNbO_3$

2009 J. Phys.: Condens. Matter 21 123201

(http://iopscience.iop.org/0953-8984/21/12/123201)

IOP PUBLISHING JOURNAL OF PHYSICS: CONDENSED MATTER

J. Phys.: Condens. Matter **21** (2009) 123201 (29pp) doi:10.1088/0953-8984/21/12/123201

TOPICAL REVIEW

Electron small polarons and bipolarons in $LiNbO_3$

O F Schirmer[1], M Imlau[1], C Merschjann[2] and B Schoke[1]

[1] Fachbereich Physik, Universität Osnabrück, D-49069 Osnabrück, Germany
[2] Helmholtz-Zentrum Berlin für Materialien und Energie GmbH, D-14109 Berlin, Germany

E-mail: schirmer@uos.de

Received 13 August 2008, in final form 17 January 2009
Published 3 March 2009
Online at stacks.iop.org/JPhysCM/21/123201

Abstract

An overview of the properties of electron small polarons and bipolarons is given, which can occur in the congruently melting composition of $LiNbO_3$ (LN). Such polarons influence the performance of this important optical material decisively. Since coupling to the lattice strongly quenches the tunnelling of free small polarons in general, they are easily localized at one site even by weak irregularities of a crystal. The mechanism of their optical absorptions is thus shared with those of small polarons localized by binding to selected defects. It is shown that the optical properties of free electrons in LN as well as those bound to Nb_{Li} antisite defects can be attributed consistently to small polarons. This is extended to electron pairs forming bipolarons bound to Nb_{Li}–Nb_{Nb} nearest neighbours in the LN ground state. On the basis of an elementary phenomenological approach, relying on familiar concepts of defect physics, the peak energies, lineshapes, widths of the related optical absorption bands as well as the defect binding energies induced by lattice distortion are analysed. A criterion universally identifying small polaron absorption bands in oxide materials is pointed out. For the bipolarons, the dissociation energy, 0.27 eV, derived from a corresponding study of the mass action behaviour, is shown to be consistent with the data on isolated polarons. Based on experience with simple O^- hole small polaron systems, a mechanism is proposed which explains why the observed small polaron optical absorptions are higher above the peak energies of the bands than those predicted by the conventional theory. The parameters characterizing the optical absorptions are seen to be fully consistent with those determining the electrical conductivity, i.e. the bipolaron dissociation energy and the positions of the defect levels as well as the activation energy of mobility. A reinterpretation of previous thermopower data of reduced LN on the basis of the bipolaron model confirms that the mobility of the free polarons is activated by 0.27 eV. On the basis of the level scheme of the bipolarons as well as the bound and free polarons the temperature dependence of the electronic conductivity is explained. The polaron/bipolaron concept also allows us to account for the concentrations of the various polaron species under the combined influence of illumination and heating. The decay of free and bound polarons dissociated from bipolarons by intense short laser pulses of 532 nm light is put in the present context. A critical review of alternative models, being proposed to explain the mentioned absorption features, is given. These proposals include: single free polarons in the (diamagnetic) LN ground state, oxygen vacancies in their various conceivable charge states, quadpolarons, etc. It is shown why these models cannot explain the experimental findings consistently.

(Some figures in this article are in colour only in the electronic version)

Contents

1. Introduction

A small polaron forms when a charge carrier is self-trapped at essentially one site in condensed matter, as induced by sufficiently strong short range interaction of the carrier with the surrounding lattice[3]. The neighbouring ions then vibrate around new, displaced equilibrium positions. The resulting energy lowering is larger than half the width of the energy band expected from tunnelling between equivalent sites in a rigid crystal. For small polarons, therefore, such tunnelling is very strongly quenched; it is dominated by the lattice distortion dragged along with the carrier. Even modest irregularities of the lattice will then cause complete localization at one site and only thermally activated hopping will allow transport to neighbouring sites. This usually encountered situation of free small polarons thus cannot be distinguished from that of bound small polarons localized by disorder in noncrystalline matter or by lattice defects in a crystal. It allows us to treat in particular the optical properties of small polarons from a common viewpoint, irrespective of whether free or bound.

Seen under this aspect, appropriately prepared lithium niobate ($LiNbO_3$, abbreviated LN) exhibits various manifestations of small polarons, free as well as bound [2], profoundly influencing the optical properties of the material. In order to deal adequately with the features of these polarons in the numerous possible optical applications of LN, mainly based on its acousto-optical, nonlinear optical, electro-optical and especially photorefractive properties [3–6], it is essential to understand their microscopic structures and the related physical properties. Electrons self-trapped at the regular Nb_{Nb}^{5+} ($4d^0$) ions of the LN lattice form the most simple polaron species, free small polarons. Second, electrons can be captured at the Nb_{Li}^{5+}($4d^0$) antisite defects ($Nb_{Li}^{4\bullet}$ in Kröger–Vink notation [7]: for the nomenclature of this and further defects, see table A.1), present as the natural, fourfold positively charged intrinsic donors in the material. These defects compensate the cation vacancies, such as the negatively charged Li vacancies V'_{Li}, which result from the Li deficit of the usually employed congruently melting composition of LN. For overviews on numerous material aspects of LN, including the preconditions leading to the specific defect structures, see the reviews and articles by Räuber [8], Weis [9] and Smyth [10, 11]. The localization of an electron at Nb_{Li}^{5+} is not only caused by the antisite defect potential but also—and to a larger extent—by the concomitant lattice distortion. This allows us to qualify the resulting object, Nb_{Li}^{4+}($4d^1$), as a bound small polaron. Third, the nearest-neighbour pairs Nb_{Li}^{5+}–N_{Nb}^{5+}($4d^0$–$4d^0$) can accommodate two electrons, which are stabilized mainly by moving the ions towards each other along the lattice mode responsible for the ferroelectricity of LN. In this way the electron pair forms a bound bipolaron, i.e. a special case of a 'negative-*U*' [12] situation, occurring if the Coulomb repulsion is overcompensated by the joint lattice distortion. The electron pair at the resulting Nb_{Li}^{4+}–Nb_{Li}^{4+}($4d^1$–$4d^1$) defect can be dissociated optically as well as thermally, and the wealth of information gained from related investigations make the couple a paradigm of small bipolarons in general. To these polarons, containing ions intrinsic to the LN lattice, one can add electrons bound to extrinsic ions, such as Fe_{Li}^{2+}; the optical absorptions of such defects are also dominated by small polaron features, analogous to those of the former Nb-based polarons. All these types of small polarons contain electrons, which are supplied by raising the Fermi level of the material by chemical or electro-chemical reduction or by appropriate irradiation. In the latter case also holes can be formed in the valence band, which subsequently are trapped by Li vacancies, V_{Li}, leading to V_{Li}–O^- bound small hole polarons. The optical properties of this and analogous O^- systems in numerous other oxide materials have been treated in [13].

The optical absorption bands of all the electron polarons studied here, Nb_{Nb}^{4+}, Nb_{Li}^{4+} and Nb_{Li}^{4+}–Nb_{Li}^{4+}, together covering

[3] For concise information also on other types of polarons see [1].

the energy range from about 0.2 to 3.5 eV, are based on the light-induced transfer of each polaron carrier out of its potential well to one of the neighbouring Nb ions. This corresponds to the established absorption mechanism proposed, refined and summarized by Reik [14, 15], Eagles[4], Klinger [17], Austin and Mott [18] and Emin [19, 20]. The optical absorption of small bipolarons has been treated by Emin [20] as well as by Alexandrov and Mott [21] and Alexandrov *et al* [22], as based on a discussion of this subject by Bryksin *et al* [23]. For a recent collection of overviews on the properties of polarons in general see also Alexandrov [24]. In the historical development of the theory of small polaron optical absorption, transitions were, sometimes implicitly, assumed to occur only from an orbital ground state at the initial site to an equivalent ground state at one final site. There is evidence [13] that the presence of several equivalent final sites in the distorted environment must also be taken into account, leading to corresponding molecular orbital type final state splittings. In addition, there are situations where transfer transitions to excited orbital states at the final sites must be considered [13]. In both cases there is an increased density of the final states at higher energies. These are thus likely to explain the experimental observation that typically only the low energy onsets of small polaron absorption bands are predicted well by assuming the original approach; usually, however, the observed absorption of small polarons extends beyond these low energy onsets [25].

The presence of small bipolarons in a material can be proved generally only by circumstantial evidence, since they tend to form a diamagnetic singlet ground state, preventing their investigation by electron paramagnetic resonance (EPR), the most compelling method to identify the geometrical, ionic and electronic structure of defects in a material. Still, various cases have been established where bipolarons determine the structural and electronic properties of insulating compounds; they include Ti_4O_7 [26], WO_3 [27], $BaTiO_3$ [28] and boron carbide ([29] and numerous references therein). In LN the bipolarons offer the opportunity that they can be dissociated optically, in addition to their thermal breaking, which allows us to study the resulting rather long-living single polarons at low temperatures. This feature is shared with bipolarons in slightly oxygen-deficient WO_3 [27]. The EPR analysis of the paramagnetic dissociation products allows us to draw conclusions on the characteristics of the bipolaron precursors, including the consistency of the bipolaron model, its presumed structure, its optical properties, the dynamics of the related dissociation and recombination processes and its binding energy [30, 31].

Previously, summarizing accounts on polarons in LN have been included in reviews on defects in LN [2] or on defects in photorefractive materials in general [32, 33]. It appears to be appropriate to present an updated review concentrating specifically on polarons in LN. Numerous new related aspects have been discovered in the mean time, complementing each other and the previous ones, when seen from the perspective of the initially proposed polaron/bipolaron model. For instance, the optical absorption features introduced in LN by short high-intensity light pulses [34] are in full accord with the model; they support it and shed new light on the polaron properties in LN and their recombination to bipolarons. Models alternative to those based on the field of polarons in LN have been and still are put forward, claiming to explain the optical and conduction properties of the material in its reduced and/or irradiated state. In these alternative approaches the difference in the defect chemistry of LN, when compared to that of the common oxide perovskites, i.e. mainly the influence of the Li deficit of congruently melting LN and the related consequences, have not been considered sometimes. The present reassessment of the phenomena outlined in these studies shows that they can essentially be attributed to the various properties of polarons. LN, with its various manifestations of polarons, thus offers itself as an excellent testing ground for small polaron physics, not only with respect to the conceptual models but also concerning their experimental realization. This study therefore also has a strong bearing on the optical and electrical applications of LN. The scientific and technical importance of the material in these fields has been seen to increase continuously during the last decades. The polaron/bipolaron model was the basis for useful photorefractive optical storage schemes [35, 36].

It has been realized rather early [37, 38] that the theoretical treatment of small polarons involves essential aspects in common with methods employed in the physics of colour centres [39–41]. The way how electron–lattice coupling is introduced in this context has become almost intuitive during the last few decades, because it is an essential topic in the usual textbooks on solid state physics. In order to exploit this familiar connection, it will also be employed in the present context as a rather flexible and universal phenomenological guideline, when looking for further insights into the properties of small polarons. The quantum-chemical modelling of the self-localization of charge carriers as small polarons and their optical absorptions appears to have become accessible only recently [42] in a reliable way; it is only by a judicious consideration of the methods employed in describing exchange correlation that self-localization among equivalent sites is described correctly [43, 44]. As expected, for example, a preponderance of Hartree–Fock type exchange tends to overestimate self-trapping, while the local density approximation underestimates it.

Finally, we contrast the electron small polarons, to which this review is devoted, to hole small polarons, present as O^- ions bound to defects, as mentioned above. They have been identified in numerous oxide materials [13], and also in LN, and consist of single holes bound to an acceptor defect, e.g. a cation vacancy. Here the hole is often localized at just one of the equivalent oxygen ions on the inner oxygen surface next to the vacancy or next to an analogous attracting acceptor ion. All polaron optical transitions, leading to strong and wide absorption bands in the visible, occur along this inner oxygen surface. In contrast, the electron bound polarons treated in the present review are localized at the defect cation itself, and polaron transitions take place to nearly equivalent cation neighbours in the compound. The experience previously

[4] A treatment of related interband transitions is presented in [16].

gained with the simple bound O^- polarons [13] is seen to be a guideline for the interpretation of the features of the present electron polarons.

This review will be organized in the following way: the properties, mainly optical, of small polarons, including bipolarons, both free and bound, will first be outlined in a general and concise way. Then the structural and chemical features which qualify LN to be the basis for the various polaron manifestations will be described. It will be shown how raising the Fermi level will result in the related polaron optical absorption bands and how they are to be interpreted, using the discussed polaron models. In a further section it will be demonstrated that extensions of the presently used models for small polaron absorptions, including excited states resulting from tunnelling between the equivalent final sites, will be likely to occur. The principles governing the relative concentrations of free single polarons, bound single and bipolarons, as depending on temperature and illumination, both triggering dissociation, and the related time-dependent recombination, will then be outlined. In this context results of previous investigations of thermopower and electron conductivity will also be proved to be fully consistent with the optical properties. The connected experimental observations constitute a strong support for the polaron/bipolaron model in LN. Also recent new insights into polaron physics in LN resulting from their investigation by short intense laser pulses will be treated. The consistency of the arguments used will be assessed by comparing them to other models put forward in the existing extended literature on the wide optical absorption bands induced in undoped LN by raising the Fermi level and related methods.

2. Principles of the optical absorption by small single polarons and bipolarons

2.1. Free small polarons

In the following a concise overview on the optical absorption mechanisms of small polarons is given. For more extended and fundamental information the reader is referred to, for example, articles by Emin [19, 20]. The related processes will be visualized by figures based on a BO plane of an ABO_3 oxygen perovskite in which one electron is self-trapped as a small polaron or two electrons as a small bipolaron. Such objects have been identified experimentally by studies based on electron paramagnetic resonance, e.g. in locally strained $BaTiO_3$ [45]; for related transport studies see Kolodazhnyi *et al* [46]. In the BO planes the translation-symmetric B cations tend to be the trapping sites for free electron small polarons. For such small polarons the electron density does not extend essentially beyond a trapping cation site, and the lattice distortion stabilizing the electron at one site mainly affects the bonds connecting the trapping site with its first neighbours (figure 2.1).

The localization of an electron raises its kinetic energy, typically by half the width of the rigid lattice conduction band. For the formation of a small polaron this energy must be overcompensated by the energy lowering due to displacements

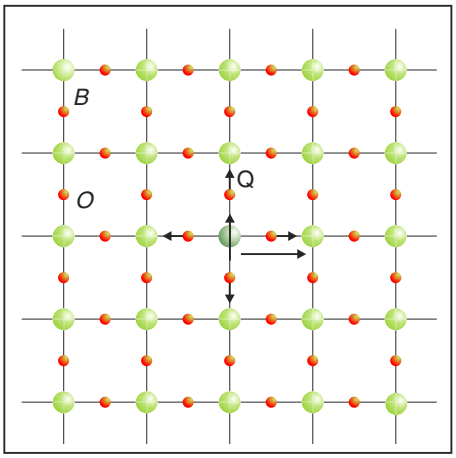

Figure 2.1. Visualization of a small electron polaron, self-localized at a B cation in a BO plane of an ABO_3 perovskite. The extra electron, symbolized by its up spin, is stabilized by repulsion mainly of its neighbouring ions, described by the interaction coordinate Q. For a small polaron the electron density is essentially confined to one cation site and the lattice distortion does not extend further than about one bond length. Optical absorption is caused by optical transfer of the electron to an equivalent cation site; transfers to one of the next neighbours occur with the highest probability. Such a transition is symbolized by the long arrow. Usually the simplifying assumption is made that the electron energy at the final site is not affected by the distortion at the initial one.

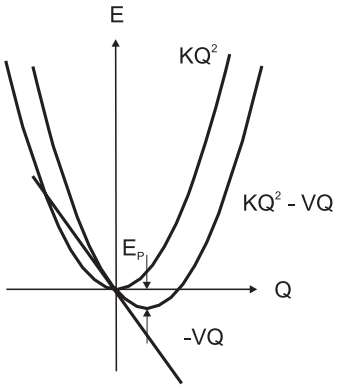

Figure 2.2. The energies contributing to the stabilization of a small polaron. The addition of an electron to the lattice repels its neighbours and the electron energy is lowered by $-VQ$. The corresponding distortion costs elastic energy, KQ^2. The sum of both contributions has a minimum energy $E_P = V^2/4K$ at $Q_{min} = V/2K$. At this distortion the electronic energy is $-VQ_{min} = -V^2/2K = -2E_P$.

of the neighbouring ions by sufficiently strong short range interactions with the lattice and, possibly, also by additional long range Coulomb forces [47, 48]. In this way the electronic energy is decreased by $-VQ$, where V is the net force on the neighbours and Q represents the distances by which they are displaced. The parameter Q can be considered to be a collection of displacements, as shown in figure 2.1. The total energy, including also the elastic energy KQ^2, which limits the distortion, is (cf figure 2.2)

$$E = KQ^2 - VQ. \tag{2.1}$$

Here the increase of the kinetic energy, by symmetry equal

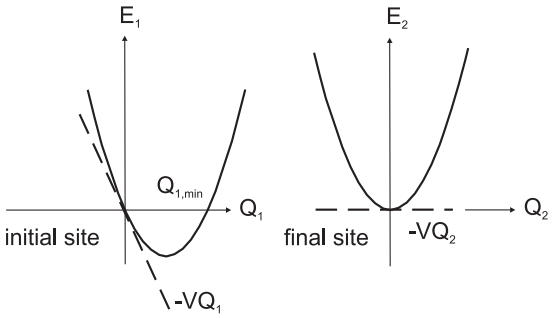

Figure 2.3. Energies of the system 'electron + lattice'. Left: electron self-trapped at a cation site; the lattice is distorted (displaced oscillator). Light-induced charge transfer transitions occur to another cation site in the lattice (right), which is not distorted in the absence of the electron. It is seen that the electronic energy at the final site is zero, independent of Q_2. The transition energy is thus only determined by the distortion at the initial site.

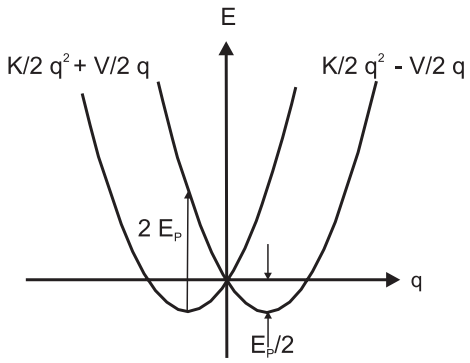

Figure 2.4. Scheme of figure 2.3, with the energies shown as depending on the relative coordinate q. Note that the curvature of the parabolas should be one half of those in figures 2.2 or 2.3.

for all possible distortion sites, has not been considered. The minimum of the energy occurs at $Q_{\min} = V/2K$ and has the value

$$E_{\min} = -V^2/4K = -E_{\mathrm{P}}. \tag{2.2}$$

The electronic energy alone is then

$$E^{\mathrm{el}}_{\min} = -V\,Q_{\min} = -V^2/2K = -2E_{\mathrm{P}}. \tag{2.3}$$

In the visible or near-infrared energy range light is absorbed directly only by electrons. Optical absorption by a small electron polaron mainly consists in a charge transfer transition of the self-trapped electron to an equivalent site (figure 2.1). The optically induced transitions occur under the condition of a 'fixed' lattice in the sense of the Franck–Condon principle. On the basis of the simplifying assumption that the stabilizing distortion at the initial site does not influence the electron energy at the final one, the energy to be expended for the photon-induced electron transfer is: $E^{\mathrm{el}}_{\mathrm{final}} - E^{\mathrm{el}}_{\mathrm{initial}} = 0 - (-V\,Q_{\min}) = 2E_{\mathrm{P}}$ (equation (2.3)). The corresponding absorption band will therefore be centred around $2E_{\mathrm{P}}$. After the light-induced electron transfer to the new site the lattice adjusts to the presence of the relocated electron. This is a spontaneous process which is not influenced by the absorbed photon. The absorption of a photon during the transfer process only serves to strip the polaron from its lattice distortion at the initial site.

In line with previous derivations of the properties of small polaron absorption bands, two items have not been considered which also tend to influence it. As seen from the absorption features of bound hole polarons in oxide materials—simple systems with well-established orbital structures [13]—both can lead to strong modifications of the small polaron optical spectra. (1) The distortion of the lattice at the initial site will usually affect also the energy of the electron at the final one. If this is neglected, the derived E_{P} is rather an upper bound of the actual one [13]. The mutual independence of sites, as far as lattice distortion is concerned, is incorporated in Holstein's linear molecule model for small polarons by construction [49]. Previous approaches to their optical absorption appear to have been based on this model. In [49] it is explicitly pointed out that neglecting the mutual influence of distortion represents an approximation. (2) Only transitions to one final site appear to have been considered, neglecting the possible excited state tunnelling among equivalent final sites. Likewise, conceivable transitions to excited orbitals at the final sites [13] have not been taken into account. As mentioned above, these mechanisms, leading to a changed density of final states, are likely to cause high energy tails of small polaron optical absorption bands, section 4.

In order to present a more intuitive visualization of the absorption and transport processes of small polarons, it is advantageous to introduce a transformation from the site-centred coordinates Q in figures 2.2 and 2.3 to those emphasizing the equivalence of initial and one final site [37, 18]. Using the site-centred coordinates, figure 2.3 shows that the presence of an electron at the initial site leads to a displaced oscillator, as shown, whereas the situation of the final site is represented by an unbiased oscillator.

The more symmetrized representation is found by the transformation [34, 18]

$$q = Q_1 - Q_2 \qquad \text{and} \qquad Q_s = Q_1 + Q_2$$

leading eventually [37, 50] to the potential sheets (figure 2.4)

$$\widehat{E} = 1/2Kq^2 \pm 1/2Vq.$$

In this transformed scheme the energy minima now occur at $q_{\min} = \mp V/2K$. They are lying below the zero level by $E_{\min,q} = -V^2/8K = -E_{\mathrm{P}}/2$. Since the vertical transition at $q_{\min}$ from the lower to the upper sheet is $4E_{\min}$, the energy of the absorption peak is again, of course, predicted to be $2E_{\mathrm{P}}$. In this alternative presentation the polaron absorption can thus be viewed as a transition between two symmetrically arranged parabolic potential sheets. Figure 2.4 also shows that the activation energy for thermally activated transport is given, essentially, by

$$E_{\mathrm{a}} = E_{\mathrm{P}}/2. \tag{2.4}$$

This is the energy of the crossing of both potential sheets above their minima. Here, at $q = 0$, the electronic energies of

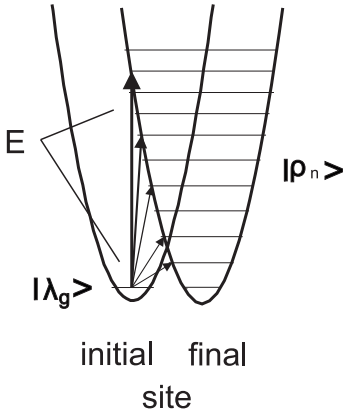

Figure 2.5. Two wells, as derived by the arguments leading to figure 2.4, exemplifying the light-induced transitions from a vibrational ground state at the initial site to any of the vibrational states at the final site.

both sites are equal, $-1/2Vq = +1/2Vq$. In this situation, which can result from appropriate thermally induced phonon excitations, a transition between both sites by tunnelling is facilitated [18, 51].

The coupling of the charge carrier to the lattice also dominates the shape of the absorption band of a small polaron. The bandwidth in this context is determined by the projections of the vibrational function at the initial site, $|\lambda\rangle$, to the possible vibrational states at the final one, $|\rho_n\rangle$: $|\langle\lambda_g|\rho_n\rangle|^2$ (figure 2.5). Here it has been assumed, for simplicity, that (a) only one representative vibration is coupled to the system and that (b) the system is studied at temperature $T = 0$, which implies that only the vibrational ground state at the initial site is populated, indicated by the subscript g. Later the modifications required for $T > 0$ will be pointed out.

It is known (see, e.g., [52, 53]) that the indicated squares of the vibration projections represent a Poisson distribution, $S^n e^{-S}/n!$, with the Huang–Rhys factor $S = 2E_P/\hbar\omega_0$, where $\hbar\omega_0$ is a representative phonon energy of the system. For strong coupling, $S \gg 1$, the envelope of the distribution can be expressed by the exponential

$$\begin{aligned}\alpha(\omega) &\propto \exp(-w(\hbar\omega - S\hbar\omega_0)^2) = \exp(-w(\hbar\omega - 2E_P)^2)\\ &= \exp(-w(\hbar\omega - M)^2) \qquad \text{with } w = 1/(2S(\hbar\omega_0)^2)\\ &= 1/(4E_P\hbar\omega_0). \end{aligned} \tag{2.5}$$

Here a peak parameter M, equal to $2E_P$ in the present situation, is introduced; it will be referred to often in the following. Up to this point a small polaron absorption band is thus represented by a Gaussian shape. A prefactor $1/\omega$ arises when treating the intensity of the absorption band, see below. Since the position of the band and its width are both completely determined by coupling to the lattice, small polaron absorption bands have the largest widths, relative to their peak energies, which are possible for homogeneous absorption bands, i.e. those arising from electronic transitions between two definite electronic levels. The ratio of the square of 'half-width at half-maximum, HWHM', W^2, over the peak energy, M, is

$$W^2/M = \ln(2)4E_P\hbar\omega_0/2E_P = 2\ln(2)\hbar\omega_0. \tag{2.6}$$

For a fixed $\hbar\omega_0$ this is a universal quantity for a small polaron absorption, independent of E_P [13]. Assuming a quantity typical for oxide crystals, $\hbar\omega_0 = 0.1$ eV, the value

$$W^2/M \approx 0.14\ \text{eV} \tag{2.7}$$

is then expected if a small polaron absorption takes place.

At temperatures $T > 0$, the width w^{-1} (equation (2.4)) of the absorption band is described by the substitution $w^{-1}(T) = w^{-1}(0)\coth(\hbar\omega_0/2kT)$ [52, 53], leading to $w^{-1}(T) = 8E_PkT$, if the thermal vibrational amplitudes dominate the zero-point excursions. For $\hbar\omega_0 = 0.1$ eV the bandwidth W increases by about 3% when raising the temperature from 0 to 300 K. The temperature dependence of W therefore has practically no influence on the characteristic quantity W^2/M. A further term proportional to $(-\exp(-\hbar\omega/kT))$, describing light emission from thermally populated final states, has to be added in principle [14, 16]. For strong coupling ($S \gg 1$), however, as valid for the systems studied here, the corresponding low energy transitions will be rather weak, and this term will thus not be considered here.

The finite transition dipole moment between initial and final sites results from a transfer mixture between the electronic parts of the wavefunctions at both sites, as indicated by the two-site Hamiltonian H, spanned by the initial $|I\rangle$ and final $|F\rangle$ states:

$$H = \begin{pmatrix} -VQ & J \\ J & 0 \end{pmatrix}. \tag{2.8}$$

Here J is the transfer energy. Assuming $J \ll VQ$, this leads to the first-order perturbed states $|I'\rangle = |I\rangle + (J/\Delta E)|F\rangle, |F'\rangle = |F\rangle - (J/\Delta E)|I\rangle$. ΔE is the distortion-induced electronic energy difference between the initial and final sites, i.e. the difference between the diagonal elements in equation (2.8). In a classical picture ΔE corresponds to the photon energy $\hbar\omega$ absorbed by the system. The expectation value of the transition dipole, $\langle I'|\vec{d}|F'\rangle$, is therefore approximately $(Jd/\hbar\omega)$. Since the energy absorption rate is proportional to $\hbar\omega|\langle I'|\vec{d}|F'\rangle|^2$ (see, e.g., [54]), the prefactor to equation (2.5) amounts to J^2d^2/ω.

The total absorption band is thus given by

$$\begin{aligned}\alpha(\omega) &\propto J^2d^2/\omega\exp(-w(\hbar\omega - 2E_P)^2)\\ &= J^2d^2/\omega\exp(-w(\hbar\omega - M)^2). \end{aligned} \tag{2.9}$$

Here, the powers of the parameters J, d and ω, characteristic for each specific system, are identical to those in the exact theory [14, 17–19].

The polarization of the absorption band is represented by the direction of the transition dipole moment $\vec{d}$, as evaluated approximately with the initial and final states $|I'\rangle$ and $|F'\rangle$. If there are several equivalent final sites, the corresponding superpositions have to be taken.

2.2. Bound small polarons

If an electron is captured by a defect ion, positively charged with respect to the replaced regular cation of a lattice, it is attracted locally by the extra potential of the defect. In addition a polaron-like stabilization by lattice distortion can occur.

We shall label such defects as bound polarons, if the optical absorption features are dominated by polaron-like transitions to next neighbours. Of course, the binding to a defect destroys the Bloch character of a free polaron, the boundary case in an ideal unperturbed lattice. However, the bandwidth of a free small polaron is so narrow theoretically [55], $\langle \hbar\omega_0 \exp(-S/2)$ (even for the most favourable, the adiabatic case $J > \hbar\omega_0$), that already modest disorder can completely immobilize such a carrier. Since the process of optical absorption of a small polaron is independent of how the localization has occurred, the absorption mechanisms are essentially identical in both cases. The extra attracting influence active in the case of a bound small polaron will, however, cause a prelocalization of the carrier already before the lattice distortion sets in. Because the potential that binds a self-trapped carrier itself depends on the distribution of the probability density of the carrier, this nonlinear behaviour will in turn cause a stronger stabilization by the prelocalization. For details see the treatment of defect-induced polaron phenomena by Emin and Holstein [48]. Therefore the distortion-related stabilization energy of a bound polaron tends to be larger than for a free one. Furthermore, the defect-induced energetic inequivalence between initial and final sites of an optical transition out of a bound small polaron will reduce the intensity of a charge transfer transition, because the mixture of initial and final site states will be more asymmetric.

Examples for bound polarons, as related to the case of $LiNbO_3$, are electrons bound to a Nb_{Li}^{5+} antisite defect, forming Nb_{Li}^{4+}. This will be treated in more detail below. The extrinsic defects Fe_{Li}^{2+}, Ti_{Li}^{3+}, etc, in $LiNbO_3$ have analogous orbital structures [56–58]. As mentioned, the absorption processes of such defects are expected to be quite similar to those of free small polarons. However, because of the defect potentials attracting the electron, in such cases the equilibrium level at the initial site is lower energetically than at the final one. This raises the peak energy and lowers the intensity of the absorption of a bound polaron as compared to a free one.

Since the initial electronic energy is now $-VQ - E_C$, where $-E_C$ is the level lowering by the defect attraction and $Q = Q_{\min}$ in equilibrium at the initial site, the absorption band is peaked at $2E_P' + E_C$, assuming again that neither the deformation at the initial site nor the defect potential influence the energy of the electron at the final site. As has been mentioned, the extra localizing effect of the defect potential will increase the polaronic coupling, as compared to a free polaron. Therefore, the polaron energy E_P' of a bound polaron will be larger than that of a free one, E_P. The bandshape is mainly determined by the coupling of the electron to the lattice; therefore the shape again is proportional to

$$\alpha(\omega) \propto 1/\omega \exp(-w(2E_P + E_C - \hbar\omega)^2) = 1/\omega \exp(-w(M - \hbar\omega)^2) \qquad \text{with } w = 1/(4E_P'\hbar\omega_0). \tag{2.10}$$

For the case of such bound small polarons the ratio

$$W^2/M = \ln(2)4E_P'\hbar\omega_0/(2E_P' + E_C) < \ln(2)2\hbar\omega_0 \tag{2.11}$$

is then expected to be somewhat smaller than 0.14 eV, the target value for free small polarons.

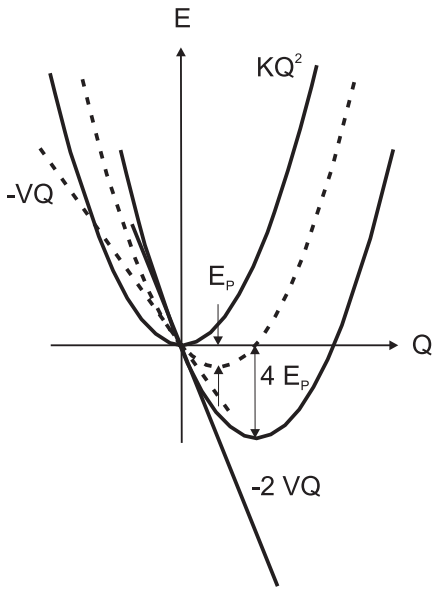

Figure 2.6. Energy model of a one-site small bipolaron, i.e. two electrons self-trapped at the same cation. The force exerted by the two electrons on its neighbours is doubled (as indicated) when compared to the case of a single small polaron. Therefore the energy of the system (full lines in the right part of the figure) is lowered by four times the polaron energy of a single polaron (dashed lines). If the excess in stabilization energy, as compared to two separated polarons, $2E_P$, is larger than the Coulomb repulsion of the two electrons, U, the bipolaron is stable.

As before (equation (2.8)), the intensity of absorption derives from a mixture between initial and final states:

$$H = \begin{pmatrix} -VQ' - E_C & J \\ J & 0 \end{pmatrix}. \tag{2.12}$$

The absorbed photon energy is now $\hbar\omega = VQ' + E_C$. The first-order transfer admixtures thus lead to the same prefactor as in equation (2.9), as shown in equation (2.10).

2.3. Free and bound small bipolarons

2.3.1. One-site free bipolaron. First the situation of a one-site bipolaron is treated. Here two electrons are self-trapped at the same cation site, attracting each other by their joint lattice distortion, see figures 2.6 and 2.7. Their Coulomb repulsion is labelled U. Since the linear response of the lattice to two electrons at one site is twice that for one electron, the total energy is now

$$E^{\text{bip}} = KQ^2 - 2VQ + U \tag{2.13}$$

having a minimum, $E_{\min}^{\text{bip}}$, at $Q_{\min} = V/K$, which yields $E_{\min}^{\text{bip}} = -V^2/K + U$. The first term is four times larger than the single polaron energy, $E_P = V^2/4K$. Using this expression, the ground state energy of the bipolaron is $E_{\min}^{\text{bip}} = -4E_P + U$. By subtracting the energy of the alternative situation, two separated polarons, stabilized by a total of $2E_P$, one arrives at the bipolaron binding energy:

$$E_{\text{bind}}^{\text{bip}} = 2E_P - U. \tag{2.14}$$

Table 1. Expressions related to the various types of bipolarons. The values of M and $E_{\rm bind}$ are available experimentally.

Bipolaron type	Free 1-site	Free 2-site	Bound 1-site	Bound 2-site
$E_{\rm total}$	$KQ^2 - 2VQ + U$	$kq^2 - 2vq + u$	$K'Q^2 - 2V'Q + U - E_C$	$k'q^2 - 2v'q + u - e_C$
$Q_{\rm min}$, $q_{\rm min}$	V/K	v/k	V'/K'	v'/k'
$E_{\rm 2electrons}$ at $Q_{\rm min}$, $q_{\rm min}$	$-8E_{\rm P} + U$	$-8e_{\rm P} + u$	$-8E'_{\rm P} + U - E_C$	$-8e'_{\rm P} + u - e_C$
M	$4E_{\rm P} - U$	$4e_{\rm P} - u$	$4E'_{\rm P} - U + E_C$	$4e'_{\rm P} - u + e_C$
$E_{\rm bind}$	$2E_{\rm P} - U = M - 2E_{\rm P}$	$2E_{\rm P} - u = m - 2e_{\rm P}$	$2E_{\rm P} - U + E_C = M - 2E'_{\rm P}$	$2e'_{\rm P} - u + e_C = m - 2e'_{\rm P}$

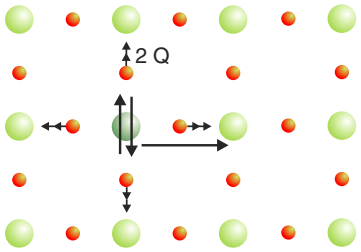

Figure 2.7. Mechanism of the optical absorption by a one-site bipolaron.

The bipolaron is thus stable [59] if the extra stabilization in the pair by joint lattice distortion, $2E_{\rm P}$, is larger than the Coulomb repulsion U.

The optical absorption of such a bipolaron proceeds by transferring one of the two electrons in the bipolaron to an equivalent final cation site (see the long horizontal arrow in figure 2.7), leaving back a (single) polaron at the initial one. The lattice around the transferred electron will adjust to its presence by forming a second single polaron. This means that the bipolaron is dissociated optically into two single polarons, assuming that they do not influence each other in their end positions.

The initial electronic energy for both electrons is

$$E_{\rm min}^{\rm bip,el} = -2VQ_{\rm min} + U = -2V^2/K + U = -8E_{\rm P} + U. \tag{2.15}$$

Here the polarization energy $2V^2/K$ is additive in the contribution of both electrons. Therefore the energy of 'electron 1' in the polaron potential well is $-V^2/K + U = -4E_{\rm P} + U$. This energy must be provided by an absorbed photon for a transfer to a final equivalent site having zero electronic energy. Here it has been assumed that the second site is sufficiently far away from the first one that the repulsion by the first electron has decayed to zero. The peak energy of the one-site bipolaron absorption, approximately being given by M, is thus expected to be observed at

$$M = 4E_{\rm P} - U. \tag{2.16}$$

This expression is identical to that reported by Emin [59], Alexandrov [21] and Calvani [60] on the basis of slightly different arguments. Comparing equations (2.14) and (2.16) it is seen that the peak energy parameter M is related to the binding energy by

$$E_{\rm bind}^{\rm bip} = M - 2E_{\rm P}. \tag{2.17}$$

All these relations are collected in the second column of table 1.

The stabilization by lattice distortion of each electron in the bipolaron can also be expressed by the Huang–Rhys factor S. The part of the electronic transition energy which is caused by coupling to the lattice is $E_{\rm bip} = S\hbar\omega_0 = 4E_{\rm P}$ in the present case. The shape of the bipolaron absorption again is given by the squared projections of the initial vibrational ground state, at $T = 0$, on the series of vibrational final states. Using the above Huang–Rhys factor in equation (2.5), this yields the width parameter $w^{-1} = 8E_{\rm P}\hbar\omega_0$, i.e. the width of the one-site bipolaron optical absorption band is expected to be larger by a factor of $\sqrt{2}$ than that of a single small polaron, for the same value of $E_{\rm P}$. One should note that the width is only influenced by lattice distortion and not by the Coulomb repulsion U, as assumed in [60].

Since the square of the width scales in the same way with $E_{\rm P}$ as the peak energy M plus U (equation (2.16)), the ratio

$$W^2/(M + U) = \ln(2)8E_{\rm P}\hbar\omega_0/4E_{\rm P} \approx 0.14\ {\rm eV} \tag{2.18}$$

is expected to be identical to that expected for single polarons. The experimentally directly accessible value, W^2/M, for free bipolarons is now predicted to be larger than 0.14 eV, because $M < M + U$:

$$W^2/M > 0.14\ {\rm eV}. \tag{2.19}$$

As in the previous cases, the bipolaron absorption derives its intensity from the admixture of the initial state of the transposed electron to that of the final one (see equation (2.8)). In first order, this admixture is $J/\Delta E$, with ΔE the energy difference of the transferred electron at the equilibrium configuration of the initial site to the undistorted final site, i.e. $\hbar\omega$. The intensity of the band thus is again proportional to $J^2d^2/\hbar\omega$:

$$\alpha(\omega) \propto J^2{\rm d}^2/\omega \exp(-w(4E_{\rm P} - U - \hbar\omega)^2)$$
$$\text{with } w = 1/(8E_{\rm P}\hbar\omega_0). \tag{2.20}$$

From fitting equation (2.20) to the experimental bipolaron absorption band, the parameters M and W (equations (2.16) and (2.18)) can be derived. As before, the polarization of the absorption is determined by the matrix elements of $\vec{d}$.

2.3.2. Two-site free bipolaron. In this case the bipolaron contains two electrons self-trapped at two neighbouring equivalent cation sites or in a bonding orbital connecting both of them, being stabilized by joint lattice distortion (figure 2.8). These objects tend to be more stable than one-site bipolarons, since here the destabilizing electron repulsion, u, is weaker

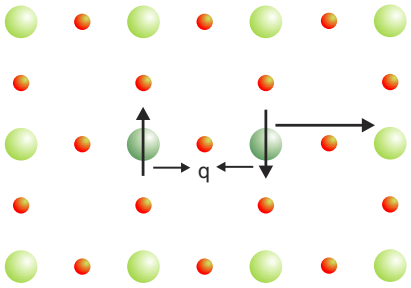

Figure 2.8. Model of a two-site bipolaron. Only the essential displacements, q, of the two bipolaron partners towards each other are indicated. They will support the homopolar binding between the two sites and thus decrease the electronic energy of the bipolaron. The light-induced transfer of one of the bipolaron electrons to an equivalent neighbour site is indicated by a long horizontal arrow.

than in the one-site case, because of the larger electron–electron distance. In addition, the stabilization of this bipolaron can profit from the formation of a molecular bond by orbitals from both sites, where the singlet state is favoured by a distortion, q, of both partners towards each other, figure 2.8.

The total energy can be modelled by

$$E = kq^2 - 2vq + u \tag{2.21}$$

with k and v the related elastic and lattice coupling parameters. Here a notation different from that concerning the one-site bipolarons is used, because the parameters can be different in the present situation. Equation (2.21) is formally identical to equation (2.13) for a one-site bipolaron, leading to equivalent expressions, see table 1.

The shape of the band is more difficult to assess than in the case of the one-site bipolaron. In the latter situation the potentials of the electrons at the site of the pair are of the same type, i.e. described by the same constants K and V, as for the transferred electron at its final site. Under this condition it is straightforward to calculate the projections of the relevant vibrational functions. The result is given above in equation (2.5). For two-site bipolarons the parameters describing the stabilizing distortion of the pair, v and k (equation (2.14)), are different from the parameters K and V related to the distortion at the final site of the isolated electron, transferred out of the pair. The projection of the initial pairing distortion on the distortion at the final site is therefore less straightforward to assess.

2.3.3. Bound bipolarons. Bipolarons can also be bound to defects. For a one-site bipolaron of this type (table 1, column 4) the energy of the partner electrons at the initial site is lowered by the attracting influence of the defect charge. If the energy of the 'first' electron is decreased by E_C, the peak energy of the optical absorption band is shifted by E_C to higher energies. Since the polaron binding energy, E'_P, is expected to be larger compared to that of a free bipolaron, there is also an increase of the peak electron transition energy because of this circumstance. Correspondingly, the width of the band, determined now by E'_P, also tends to be larger. For a free bipolaron the ratio W^2/M was expected to be higher than 0.14 eV; see the discussion leading to equation (2.19). There the parameter M fulfils $M < M+U$. For a bound bipolaron the corresponding relation is $M < M+U-E_C$. Since $E_C > 0$, M is correspondingly larger, leading to W^2/M closer to 0.14 eV.

For a two-site bound bipolaron (table 1, column 5), likely to occur in LN (see section 3), one of the binding cations ($\mathrm{Nb_{Li}}$) is a defect ion with a different attracting charge. The ground state of such a two-site bipolaron, populated by two antiparallel electrons, is characterized by a molecular orbital, comprising contributions from both sites, with a preponderance of electron density at the more attracting one. The onset of the optical absorption band will be determined by the optical transfer from this molecular orbital state to the final site. Because of the accumulation of electron density near the more attracting defect site in the bipolaron, it will be reasonable to approximate the optical absorption by the expressions valid for the one-site bound bipolaron.

Since the electron–electron repulsion increases with localizing both electrons near one site, a defect partner in a bipolaron will tend to destabilize it, even if part of the repulsion is compensated by the extra attraction by the defect. This tendency to pair breaking will allow that defect ions can be expected to be observed in isolation, even if their orbital structure would favour bipolaron formation. This appears to be the case for $\mathrm{Fe_{Li}^{2+}}$ in LN, having a ground state orbital structure topologically equivalent [56] to the bipolaron forming $\mathrm{Nb_{Li}^{4+}}$.

2.4. The DC conductivity of free small polarons

It is an intrinsic feature of small polarons that their contribution to the electrical DC conductivity is determined in all practical cases by hopping between equivalent sites. In order to accomplish this, thermally induced fluctuations of the surrounding lattice have to create situations in which the electron energies at the initial and the final sites are equal. This facilitates the tunnelling of the electron between both sites in the related thermally excited state of the crystal [51]. After the transfer, the lattice around the final site relaxes in such a way that the polaron forms again. The hopping energy, activating the mobility of small polarons, is then the minimum energy needed to establish the lattice distortion leading to the coincidence of the involved electronic energies. For free polarons this mobility activation energy, E_μ, is (see, e.g., [18])

$$E_\mu = E_\mathrm{P}/2 \tag{2.22}$$

see figure 2.4. A more detailed discussion [18] takes into account that tunnelling between initial and final sites, occurring in the situation of energy coincidence, can lead to a corresponding splitting, lowering the barrier by a transfer parameter J. Then

$$E_\mu = E_\mathrm{P}/2 - J. \tag{2.23}$$

Here the full transfer energy, J, enters in the case of adiabaticity, i.e. $J > \hbar\omega_0$, implying that the transferred electron can instantaneously adjust to the actual ionic positions. In the opposite, nonadiabatic, situation, the transfer correction to E_μ is smaller.

Table 2. Reaction energies of processes leading to intrinsic defects in $LiNbO_3$, as determined from shell model investigations [64].

(a) *Incorporation of Li deficit during crystal growth*
Compensation of V'_{Li} by $Nb^{4\bullet}_{Li}$ needs 1.26 eV less per Li_2O than compensation by $V^{\bullet\bullet}_O$
The first reaction, as an example, means: From the '$LiNbO_3$' melt 1 $LiNbO_3$ molecule plus 5 Li_{Li} are consumed to form 3 Li_2O (evaporating) as well as 1 $Nb^{4\bullet}_{Li}$ and 4 V'_{Li} (in the final crystal)

Incorporation of Li deficit	Reaction	Energy per Li_2O
By $Nb^{4\bullet}_{Li}$ antisite formation	'$LiNbO_3$' $\leftrightarrow 3Li_2O + 4V'_{Li} + Nb^{4\bullet}_{Li}$	4.56 eV[a]
By formation of $V^{\bullet}_O$	'$LiNbO_3$' $\leftrightarrow Li_2O + 2V'_{Li} + V^{\bullet\bullet}_O$	5.82 eV

(b) *Comparison of 'normal' versus ilmenite $LiNbO_3$ lattice energies*
Ilmenite is only marginally less stable than 'normal' $LiNbO_3$

'Normal' versus ilmenite $LiNbO_3$	Difference of lattice energies per unit cell	Experiment [65]
'Normal'–ilmenite	'Normal' more stable by 0.1 eV	0.1 ± 0.04 eV

(c) *Chemical reduction*
In Li deficient $LiNbO_3$ the formation of $Nb^{4\bullet}_{Li}$ needs 0.63 eV less per created conduction band electron than the formation of $V^{\bullet\bullet}_O$
First reaction, as example: from a $LiNbO_3$ crystal, containing V'_{Li}, 1 molecule $LiNbO_3$ plus 1 L_{iLi} are consumed; 1 O_2 plus 1 Li_2O evaporate. 1 V'_{Li} is filled by Nb, forming 1 Nb_{Li}; 4e′ in conduction band

Chemical reduction	Reaction	Energy per electron
Formation of $Nb^{4\bullet}_{Li}$ as donor	'$LiNbO_3$' $\leftrightarrow O_2 + Li_2O + Nb^{4\bullet}_{Li} + 4e'$	2.80 eV[b]
Formation of $V^{\bullet\bullet}_O$ as donor	'$LiNbO_3$' $\leftrightarrow O_2 + 2V^{\bullet\bullet}_O + 4e'$	3.43 eV

[a] Li_2O outdiffusion from ilmenite $LiNbO_3$ needs only 3.8 eV per Li_2O.
[b] Indiffusion of Li_2O into V'_{Li} in ilmenite part decreases the energy per electron further [64].

Using the parameter E_μ the conductivity of free small polarons is described by

$$\sigma = en\mu = en\mu_o \exp(-E_\mu/kT)/T^x, \qquad (2.24)$$

where $x = 1$ applies for the case of adiabaticity, $x = 3/2$ otherwise [55].

3. Application of the general principles to polarons in $LiNbO_3$

3.1. Structural preconditions for the formation of polarons and bipolarons in $LiNbO_3$

Although the composition of $LiNbO_3$ (LN) is formally identical to that of the common oxide perovskites, ABO_3, for instance $KNbO_3$, LN shows singular defect-related properties not found for the oxide perovskites (OP). Many of these features can be traced to the fact that Li^+ has a rather small radius (76 pm [61]), whereas K^+ in $KNbO_3$ covers much more space (138 pm), see ion A in figure 3.1. In addition both Nb and Li are surrounded by (trigonally distorted) octahedra of six oxygen ions, whereas K^+ (ion A in figure 3.1) is twelvefold-coordinated. Some of the consequences for the defect structure of LN are listed in the following.

Both the comparable ionic radii (Li^+: 76 pm, Nb^{5+}: 64 pm) and the similar surroundings facilitate the replacement of Li by Nb, forming the antisite defect $Nb^{4\bullet}_{Li}$ (electronic configuration $4d^0$) [62]. Its positive charge must be compensated; usually four negatively charged Li vacancies, V'_{Li}, are assumed to serve this purpose. This leads to the composition $[Li_{1-5y}Nb_y]_{Li}Nb_{Nb}O_3$. For congruently melting crystals the Li mole fraction $x = [Li]/([Li] + [Nb])$ is equal to 0.484 [63], by definition of the term 'congruent' identical for

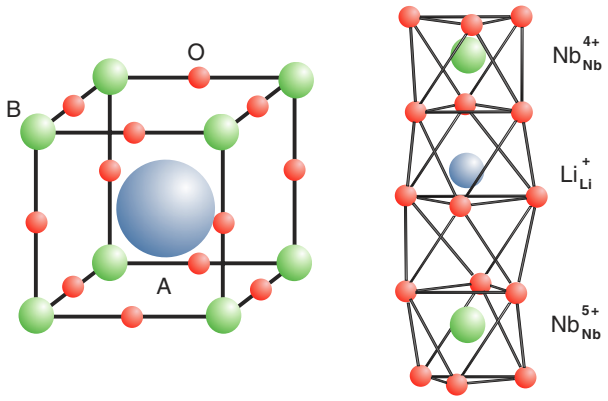

Figure 3.1. Comparison of the arrangement of A, B and oxygen ions in an ABO_3 perovskite (left) and in $LiNbO_3$ (right).

the melt and for the crystals grown from it. This corresponds to an antisite concentration, y, of about 1%. The alternative that the V'_{Li} acceptors are rather compensated by oxygen vacancies $V^{\bullet\bullet}_O$ is disproved by density measurements of the as-grown congruently melting material [62] as well as by shell model calculations (see table 2, part a) [64]. This behaviour is in contrast to that of the ABO_3 perovskites, where formation of oxygen vacancies is the most favourable compensation mechanism.

It is remarkable that the highly defective composition of LN is more stable than the stoichiometric one. The melting temperature of the congruently melting and the stoichiometric modifications are, resp., 1253 and 1164 °C. This shows that, quite surprisingly, the presence of intrinsic defects stabilizes the structure. Also the large phase width of compositions crystallizing in the LN structure, $0.44 < x < 0.50$, is a

consequence of defect incorporation. So, LN is a defective material par excellence. Only under special growth conditions can stoichiometric crystals be obtained (for an overview, see [5]).

The comparable sizes of the Li^+ and Nb^{5+} ions, facilitating their exchange, may also be one of the reasons why the 'proper' LN configuration (figure 3.1) and the LN ilmenite structure have almost the same lattice energies (table 2, part b). In the latter case the cation sequence along the axis, replacing that in figure 3.1, is . . . Nb–Li—structural vacancy—Li–Nb . . .. Such a structure corresponds to a correlated cumulation of Nb_{Li} antisite defects. Its importance for the scenario of intrinsic defects in LN has been recognized by Smyth [11]. This configuration could indeed be prepared in a low temperature process by Mehta *et al* [65] and was found to be less stable than the normal $LiNbO_3$ structure by a small amount of only about 9.8 ± 4.1 kJ mol^{-1}. Donnerberg *et al* [64] (see table 2, part b) had predicted 0.1 eV per unit cell (9.6 kJ mol^{-1}) theoretically. Therefore it is likely that some ilmenite LN intergrowths are solved in the actual high temperature grown LN crystals.

If an Li ion is missing in an ilmenite cation sequence, the site of this Li vacancy can correspond to that of an Nb vacancy, as referred to the normal LN sequence. This change of the reference basis is able to solve the problem that—on the one hand—the occurrence of vacancies at normal Nb sites, V_{Nb}, has been inferred from x-ray diffraction studies by Abrahams and Marsh [66], while—on the other hand—the formation of an Nb vacancy in the normal LN cation sequence requires a very high energy [64]. The creation of an Li vacancy in an ilmenite sequence, which can be related to an Nb vacancy in the normal sequence, requires less energy (table 2). Since reference to cation vacancies in the present context occurs only with respect to their potential for charge compensation, we shall continue, for the sake of simplicity, to label them as V'_{Li}, irrespective of their localization in an ilmenite or a normal LN cation sequence.

The ease of Li and Nb exchange in Li-deficient LN also promotes the diffusivity of Nb. Nb ions transported into the crystal in the reduction process (table 2, part c) can move to their final sites by hopping from Li vacancy to Li vacancy, followed by a site change at the end of the diffusion path. A lack of Li vacancies thus impedes the reduction process, as observed: reduction conditions leading to strong coloration in congruently melting material are almost inefficient for nearly stoichiometric crystals [67].

Table 2 furthermore shows, in part c, that also under chemical reduction the formation of additional $Nb^{4\bullet}_{Li}$ is more favourable than of $V^{\bullet\bullet}_O$. The compensating conduction band electrons are then trapped at $Nb^{4\bullet}_{Li}$, giving rise to the manifestations of small electron polarons to be discussed in the following.

The formation of Nb_{Li} antisite defects during crystal growth can be decreased or even avoided by adding high concentrations of $Mg^{\bullet}_{Li}$ or other donors to the melt, which have a higher ionic binding energy at the Li site than the Nb antisite defect (Nb_{Li}) [6]. If such donors lead only to shallow trap levels, already ionized at low temperatures, the

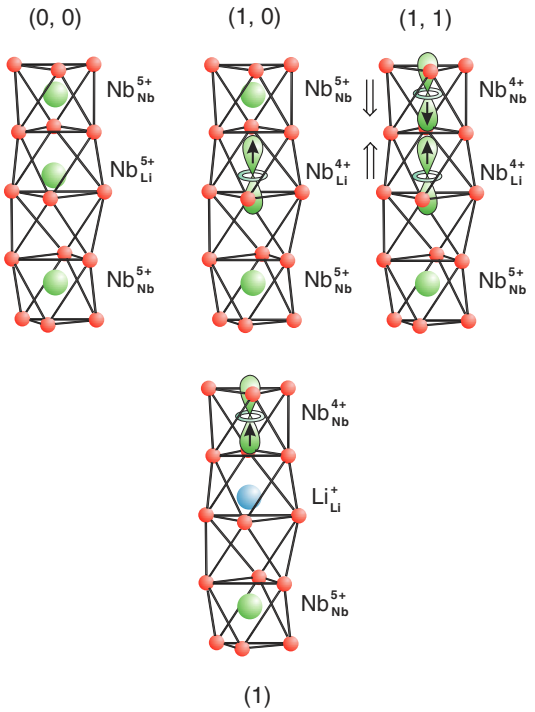

Figure 3.2. Visualization of the orbital ground states of the Nb^{4+} ions forming polarons in LN. The orbitals shown are stabilized by the locally active crystal fields. Upper part left: (0, 0)—pairs of neighbouring Nb_{Nb} and Nb_{Li} ions, holding no electron. The corresponding electron configurations are ($4d^0$). Centre: (1, 0)—one electron: Nb^{4+}_{Li} ($4d^1$) bound polaron, P. Right: (1, 1)—two electrons: $Nb^{4+}_{Li} - Nb^{4+}_{Li}$ ($4d^1$–$4d^1$) bound bipolaron, B. The two vertical double arrows indicate the relaxation of the Nb ions towards each other, increasing the bipolaron binding energy. Lower part: (1)—one electron at Nb^{4+}_{Nb}: free small polaron.

polaron trapping behaviour of such specially doped LN crystals then approaches that of the typical ABO_3 perovskites: added electrons are accommodated in the conduction band, leading to isolated Nb^{4+}_{Nb} ($4d^1$) free polarons.

In addition to chemical reduction, also solid state electrolysis [68, 69] allows us to raise the Fermi level in such a way that the Nb polaron states are occupied. Furthermore, one-photon optical absorption, exciting electrons from extrinsic defects, such as Fe^{2+}_{Li}, to the conduction band, or two-photon absorption, exciting valence band electrons, can populate the polaron states. The holes formed in the valence band by the latter method tend to be captured near Li vacancies, V'_{Li}, forming $O^- – V'_{Li}$ hole small polarons [13]. Also x-ray irradiation can create electron and hole small polarons [70].

Figure 3.2 indicates the small polaron orbital structure resulting from trapping conduction band electrons at the Nb^{5+}_{Li} ($4d^0$) antisite defects, leading to Nb^{4+}_{Li} ($4d^1$), labelled (1, 0) in figure 3.2. The first cation neighbours of an antisite defect are Nb^{5+}_{Nb} ($4d^0$), i.e. Nb ions on normal lattice sites. Such nearest-neighbour pairs of identical cations at inequivalent sites are absent in the typical oxide perovskites. An Nb_{Nb}–Nb_{Li} bond can form between these two Nb ions, if occupied by two electrons, forming (1, 1) in figure 3.2. Since the electronic ground state of Nb^{4+}_{Li} ($4d^1$), i.e. the antisite defect having trapped one electron, has ($3z^2$–r^2)-type nearly axial

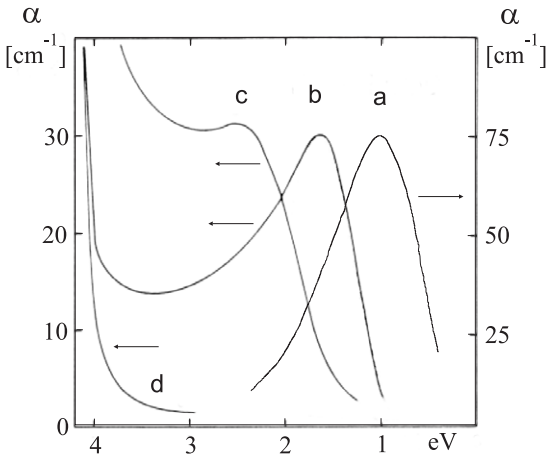

Figure 3.3. Schematic overview of the optical absorption bands caused by electron polarons and bipolarons in LN [33]: (a) F(1): free Nb^{4+}_{Nb} polaron. (b) $P(1, 0)$: bound Nb^{4+}_{Li} polaron. (c) $B(1, 1)$: bound bipolaron Nb^{4+}_{Nb}–Nb^{4+}_{Nb}. (d) Untreated crystal.

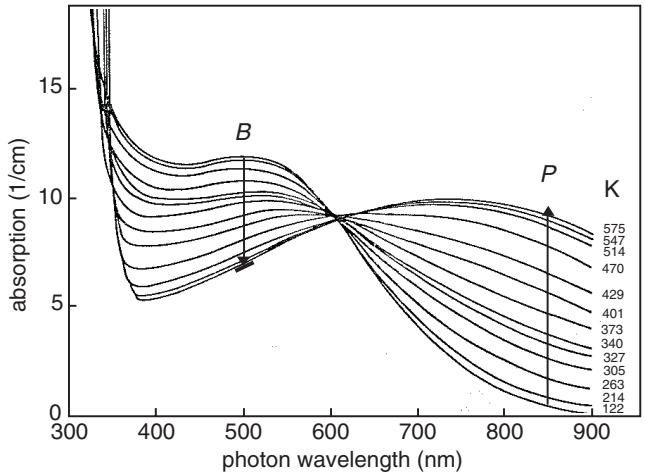

Figure 3.4. Thermal dissociation of bipolarons B into bound polarons P [75]. The process follows the reaction $B \leftrightarrow P + P$ reversibly. The existence of the isosbestic point indicates that the reaction is described by only one double arrow, as shown, without any side reaction. The temperature-dependent absorption changes near 350 nm reflect the temperature dependence of the fundamental absorption.

symmetry with respect to the trigonal axis [71] and since the same can be expected for Nb^{4+}_{Nb} ($4d^1$) [72], the orientation of the 'Nb–Nb' molecule along the axis will be most stable; along this direction the orbital overlap is strongest [64, 71]. The formation of Nb^{4+}_{Li}–Nb^{4+}_{Nb} bipolarons with the Nb–Nb directions lying perpendicular to the c axis, as proposed by Dutt *et al* [73], is thus not expected. The strength of the bonding increases, if both ions relax towards each other [64], as indicated by the arrows next to (1, 1) in figure 3.2. This is similar to the situation in an H_2 molecule, which has a ground state molecular orbital with a stronger binding and a shorter bond distance than H_2^+. Finally, the self-trapping of a conduction electron in LN, in which the presence of Nb_{Li} antisite defects has been avoided by adding more than about 6% Mg or Zn to the melt, leads to the configuration labelled (1) in figure 3.2. As will be shown, in this situation the conduction electrons LN exhibit the properties expected from a free small polaron.

In passing, it is noted that the $(3z^2–r^2)$ orbital structure of the Nb^{4+}_{Nb} and Nb^{4+}_{Nb}–Nb^{4+}_{Li} ions in figure 3.2, inferred from EPR studies, is identical to that predicted by first-principles calculations of the lowest conduction band states of ideal defect-free rigid LN [72]. As part of a small polaron, such an orbital is further stabilized by short range coupling to the lattice. Such interactions have not been included in [72]. Since the formation of small electron polarons will lower the conduction band edge below the rigid lattice prediction, their existence might explain why Schmidt *et al* [72] calculate a considerably larger bandgap than that found experimentally.

Very recently the electronic and ionic structures of the bound polarons $Nb^{3\bullet}_{Li}$ and bound bipolarons ($Nb^{3\bullet}_{Li}$–$Nb^{4\bullet}_{Nb}$) have been simulated by first-principles investigations [74]; the results confirm the anticipated models shown in figure 3.2. It is found, in particular, that there is a strong relaxation of the partner ions in the bipolarons towards each other with a preponderance of electron density near the more attracting Nb_{Li} site.

3.2. Experimental data on the optical polaron phenomena in $LiNbO_3$

Following a corresponding rise of the Fermi level in congruently melting undoped LN, the band $B(1, 1)$, (c) in figure 3.3, peaked near 2.5 eV, appears. The band is attributed to bipolarons, labelled (1, 1) in figure 3.2, based on the following observations: by raising the temperature of a crystal which exhibits this band at 2.5 eV, the absorption $P(1, 0)$, peaked at 1.6 eV, increases, assigned to the model (1, 0) in figure 3.2. The phenomenon can be interpreted as a thermal dissociation of bipolarons: $B \leftrightarrow P + P$. These results were inferred from optical absorption measurements of a sample kept in vacuum ('*in situ measurements*'), while the temperature was changed as indicated [75] (figure 3.4).

It was shown that the corresponding law of mass action is fulfilled, indicating that there is an equilibrium of the relative concentrations of B and P, depending only on temperature (in the absence of illumination) (figure 3.4). The reaction is activated by an energy $\varepsilon_b = (0.27 \pm 0.02)$ eV [75], corresponding to the dissociation energy of the two electrons in the bipolaron. This process can also proceed optically under illumination with photon energies lying in the existence range of the band $B(1, 1)$; the dissociation efficiency, however, rises with increasing photon energy [76, 73]. That only the components B and P are involved in the process is demonstrated by the presence of an isosbestic point at $\lambda = 605$ nm in figure 3.4; this indicates that no conceivable further competing reaction beyond $B \leftrightarrow P + P$ is involved. Here it should be considered that this relation describes only the net reaction. It is a specific feature of 'negative-U' systems [12], including bipolarons, that their thermal dissociation leads to a simultaneous ejection of two carriers: if the mean thermal energy in a crystal is high enough to ionize the 'first', more strongly bound, electron this energy is *a fortiori* sufficient

to eject also the second one, since its 'attracting' partner is missing. This means that free polarons F are expected to occur at first under thermal dissociation: $B \rightarrow F + F$; these F are recaptured very fast and then form P, and eventually B, again. Also under optical dissociation at low temperatures, at least the reaction $B \rightarrow P + F$ should occur. In all cases, however, the recombination $F \rightarrow P$ occurs so rapidly that the presence of F could be monitored only by elaborate time-resolved measurements.

In more detail, figure 3.4 shows the temperature dependence of the total absorption, i.e. the sum $S(\lambda, T)$ of the polaron and bipolaron bands. This superposition can be expressed as $S(\lambda, T) = b(T)B(\lambda) + p(T)P(\lambda)$, where the temperature-dependent weights of the bands are $b(T)$ and $p(T)$, resp., and $B(\lambda)$ and $P(\lambda)$ are the wavelength-dependent bandshapes. In sections 3 and 4 mainly the physical interpretation of these bandshapes $B(\lambda)$ and $P(\lambda)$ will be addressed, while the reaction dynamics, determining the weights $b(T)$ and $p(T)$, will be evaluated in section 5. These weights are evaluated from figure 3.4 by following the vertical arrows for the indicated temperatures. The values of $p(T)$ are proportional to the increase of the absorption at 850 nm, starting from its low temperature value, 122 K, being given by the rather small low temperature absorption of $B(850\ \text{nm})$ at this wavelength: $p(T) = (S(850\ \text{nm}, T) - B(850\ \text{nm})b(122\ \text{K}))/P(850\ \text{nm})$. Certainly, the value of $b(122\ \text{K})$ will decrease by raising the temperature. But since $B(850\ \text{nm})$ is rather small, this change is only weighted by the corresponding low initial absorption; this contribution will therefore be neglected at all temperatures. The values of $b(T)$ are determined at 500 nm, where $b(T)$ has its maximal value at 122 K. By raising the temperature, $b(T)$ decreases but the value $b(T) = 0$ is reached only asymptotically. The value of the total absorption $S(500\ \text{nm})$, which would correspond to $b(T) = 0$, has been inferred from an independent experiment in which the bipolaron concentration was set to zero by complete optical dissociation at 80 K. The resulting total absorption, indicating $P(500\ \text{nm})$, is marked by the short line at which the arrow at 500 nm ends.

Bipolarons tend to form a diamagnetic singlet ground state, preventing a direct proof of their existence using paramagnetic resonance methods. On the basis of circumstantial evidence and of consistency arguments, we shall show, however, that the 'polaron/bipolaron' model is the only one which can account—qualitatively as well as quantitatively—for all related observations. The thermal and optical dissociations of B, see figure 3.4 and further information below, are strong arguments in this context. A metastable optical dissociation of bipolarons was first reported for such objects in slightly reduced WO_3 [27]. In the present case the structure of the emerging defect P has been shown, using electron paramagnetic resonance [71], to have a ground state as indicated under (1, 0) in figure 3.2. It has the character of a 4d orbital with $(3z^2–r^2)$ type symmetry (A_1 in the—approximate—symmetry C_{3v}); its axis is tilted by about 10° with respect to the direction of the c axis in glide-mirror planes, i.e. those containing neighbouring cations in the LN structure [71]. This deviation is probably caused

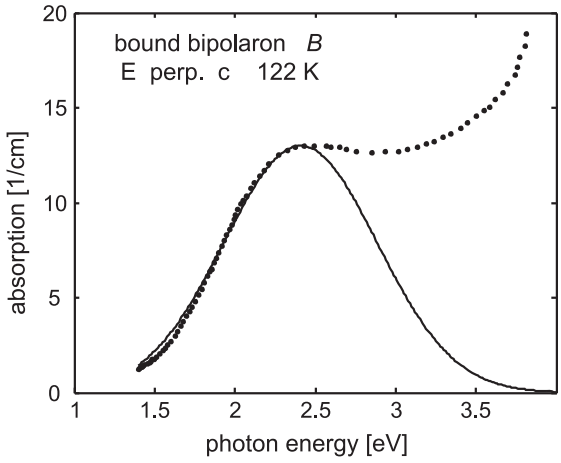

Figure 3.5. Optical absorption of congruently melting LN after reduction at 800 °C in vacuum for 1 h, band $B(1, 1)$ [75]. Ordinary polarization, $T = 122$ K. The curve fitted to the low energy onset of the band is predicted on the basis of the one-site bound bipolaron model, used as an approximation (see the end of section 2.3). For the explanation of the discrepancy between experiment and prediction at the high energy side see section 4.

by the presence of one of the intrinsic defects characteristic for congruently melting LN, probably V'_{Li}. Using optically detected magnetic resonance (ODMR), Reyher *et al* [76] have given compelling evidence that the mentioned EPR signal describes the ground state of the optical transition responsible for the band $P(1, 0)$. Other models, involving oxygen vacancy-related defects, have been proposed as an alternative to explain the bands $B(1, 1)$ and $P(1, 0)$. These concepts will be shown in section 6 to be in conflict with various observations on Li-deficient LN having a high Fermi level. Additional support for the polaron/bipolaron model will be pointed out at numerous further points in this review.

In figure 3.5 the optical absorption of congruent LN in its 'as-reduced' state, causing the band $B(1, 1)$, is seen in more detail.

Figure 3.6 shows the band $P(1, 0)$. The spectrum was obtained by illumination of a reduced specimen initially only exhibiting the band $B(1, 1)$ (figures 3.3 and 3.5) at 80 K with the unfiltered output of a 150 W xenon arc lamp. At such low temperatures the light-induced dissociation of bipolarons results completely in the bound polarons $P(1, 0)$. The peak energies of bands B and P are independent of polarization; for ordinary polarization the absorptions are slightly higher.

While figure 3.4 demonstrates the thermal dissociation of the bipolarons, figure 3.7 depicts the effect of the optical absorption changes following their optical dissociation, here with an abscissa pointing to rising photon energy. The shown difference spectrum (absorption after illumination with wavelengths 760 nm and 365 nm, resp., minus absorption before illumination) is in line with the dissociation model: the $P(1, 0)$ band rises, while the $B(1, 1)$ band decreases. Among these, the $B(1, 1)$ band extends far from its peak, 2.5 eV, up to the fundamental absorption. It may comprise a series of transitions, but these all start from the same ground state and thus are changed by constant relative weights, if their common ground state is removed by dissociation, as observed.

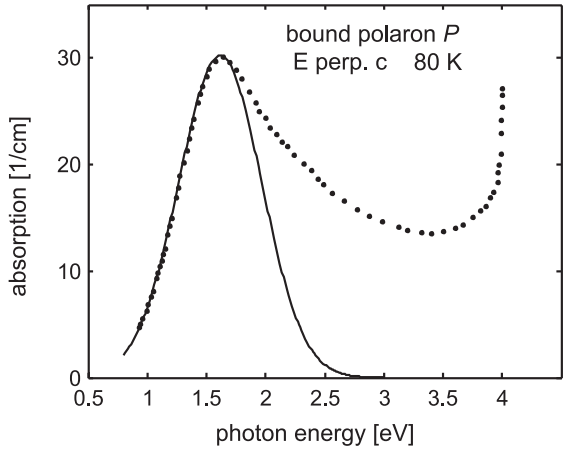

Figure 3.6. Optical absorption of electron polarons bound to the Nb_{Li} antisite defect, $P(1, 0)$ [77]. The band was observed after reduction at 900 °C in vacuum and subsequent illumination with the unfiltered output of a 150 W xenon arc lamp. The curve fitted to the low energy onset of the band corresponds to the prediction on the basis of the bound polaron model outlined in the text. The experimental high energy tail below the fundamental absorption edge will be discussed in section 4.

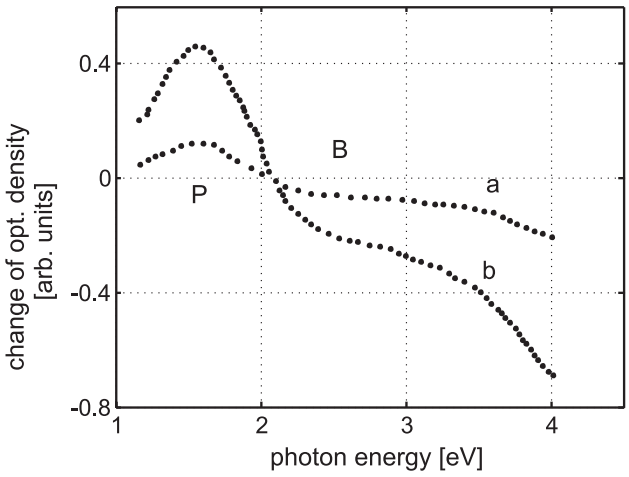

Figure 3.7. Light-induced absorption changes of a reduced congruent LN crystal, initially showing the bipolaron band B [75]. This is the equivalent of the thermally induced absorption changes, figure 3.4, now shown on an energy scale. a: response to illumination with 760 nm light; b: 365 nm light. In both cases the P band, peak at 1.6 eV, increases, whereas the B band, responsible for the absorption change at high energies, decreases.

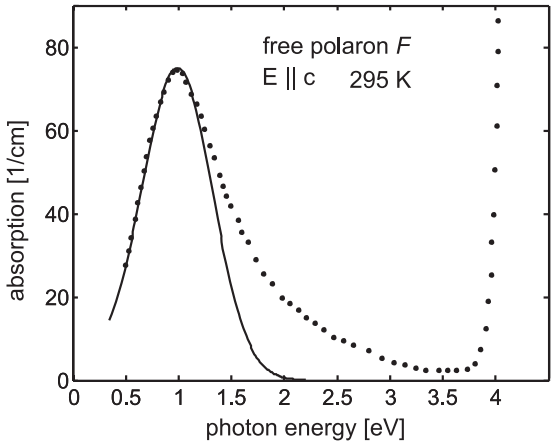

Figure 3.8. Optical absorption of the free polaron, Nb_{Nb}^{4+}, created by reduction of an LN crystal, grown from a congruently melting composition doped with 7.25% ZnO [50]. It is seen that the basic theory (equation (2.9)) (full line) reproduces the absorption at energies up to the peak energy. For a discussion of the deviation at higher energies, lower than the fundamental absorption, see section 4.

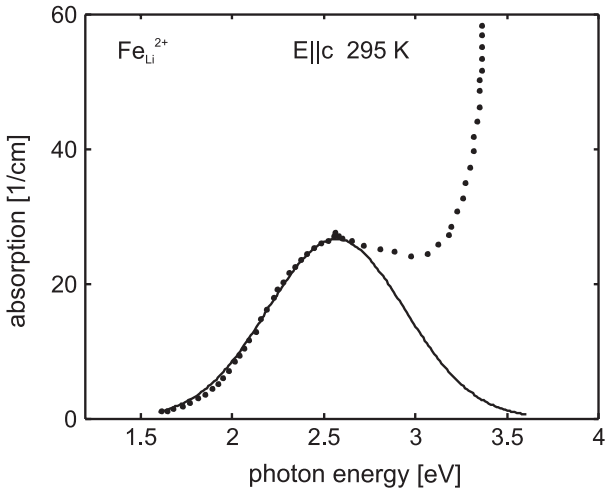

Figure 3.9. Optical absorption of Fe_{Li}^{2+} [78], a polaronic defect isoelectronic to the bound polaron Nb_{Li}^{4+}. Extraordinary polarization. The weak absorption structure, superimposed at 2.55 eV, is due to forbidden crystal field transitions within the simultaneously present Fe^{3+} ions.

Next, in figure 3.8 the absorption band of Nb_{Nb}^{4+} ($3d^1$) is shown, obtained with LN grown from a melt containing 7.25% of ZnO and subsequent reduction. As will be demonstrated, the peak energy at 1 eV, lower than that of a bound polaron, points to a free polaron as the origin of this absorption. As in the previous cases the absorption of F extends to higher energies, beyond the energy of the small polaron prediction. This will be discussed in section 4. Also their absorption is nearly independent of polarization; here the intensity is somewhat larger for extraordinary polarization [50].

The defect ion Fe_{Li}^{2+} has a $(3z^2–r^2)$-type orbital ground state. This follows from the Hund type $(3d^6) = (3d^5)(3d^1)$ ground state configuration of the ion. Here the first five electrons in the (d^5) subshell are totally symmetric, whereas the remaining $3d^1$ electron adjusts to the local crystal field, leading to an A_1 $(3z^2–r^2)$ orbital symmetry in the approximately prevailing C_{3v} type local environment [56], analogous to the previous objects, figure 3.2. Therefore it is not astonishing that it leads to a similar absorption spectrum (figure 3.9).

3.3. Analysis of the optical polaron phenomena in reduced $LiNbO_3$

In the following tables 3 and 4 the data characterizing the optical features reported in section 3.2 and their interpretation in terms of the parameters defined in section 2 are summarized.

Table 3. Parameters related to the peak energies, M, and the widths, W, of the various single polaron absorption bands. Also the parameters derived from these data on the basis of the theory developed before are given. The derivation of these data is discussed in the following.

Type of polaron	Parameter M[a] (eV)	Parameter W[b] (eV)	Derived parameter[c] E_P or E'_P (eV)	Derived parameter[c] E_C (eV)	Derived parameter W^2/M (eV)
F: free pol. (Nb^{4+}_{Nb})	1.09	0.37	0.54	0	0.13
P: bound pol. (Nb^{4+}_{Li})	1.69	0.40	0.58	0.53	0.09
Fe^{2+}_{Li}: pol. bound to Fe^{3+}_{Li}	2.62	0.44	0.70	1.22	0.07

[a] Fitted parameter M, related to the peak energy. Interpretation: $M = 2E_P$ for free polarons, $M = 2E'_P + E_C$ otherwise.
[b] $W = \sqrt{\ln(2)/w}$ with width parameter w fitted to experiment. Interpretation: $W = \sqrt{\ln(2) * 4E'_P * \hbar\omega_0}$.
[c] E'_P (for bound polarons) derived from W.

Table 4. Parameters characterizing the absorption of the bound bipolarons B, M and W are related to the peak energy and width of the band, resp. Also the parameters derived from these data on the basis of the theory developed before are given.

Parameter M[a] (eV)	Parameter W[b] (eV)	Derived parameter[b] E'_P (eV)	Derived parameter[a] $E_C - U$ (eV)	Observed bipolaron binding energy[c] ε_b (eV)	Derived parameter W^2/M (eV)
2.50	0.55	0.55	0.30	0.27	0.12

[a] $M = 4E'_P + E_C - U$.
[b] $W = \sqrt{\ln(2) * 8E'_P * \hbar\omega_0}$.
[c] $\varepsilon_b = M - 2E_{Pstab}$.

The data include the values of M and W, related to the peaks and widths of the absorption bands. In fact, M and W are defined in the theoretical expression for the absorption bands (equation (2.10)): $M = 2E'_P + E_C$ and $W^2 = \ln(2)4E'_P\hbar\omega_0$. Since in addition to the Gaussian part, equation (2.10) also includes the prefactor $1/\omega$, the fitted parameters M tend to be somewhat larger than the peak energies of the absorption bands. The widths W are the fitted half-widths at half-maximum (HWHM), representing the low energy onsets of the bands. These onsets are typical for conventional small polaron absorptions, characterized by transitions from the ground state at the initial site to an equivalent ground state at the final site. The discrepancies at higher energies in figures 3.5, 3.6, 3.8 and 3.9, on the other hand, between prediction and observation, are expected to be caused partly by further final densities of states, as discussed in section 4.

In the evaluation of the experimental data in tables 3 and 4 two assumptions had to be made: (1) the energy of the coupling phonon was assumed as $\hbar\omega_0 = 0.1$ eV. Previous investigations of small polaron optical absorptions in oxide materials [13] have shown that this is a reasonable choice. (2) Some arbitrariness is involved in the fitting of the low energy onsets. They were selected in such a way that the experimental and the fitting maxima coincided. These choices should be taken into account, when considering the quality of the derived data.

As a first result of the analysis, it is recognized that the observed relations between the values M and W, which are available without further evaluation as the parameters leading to the fits to the low energy band onsets, are typical for small polarons. For the ratio W^2/M a value of 0.14 eV is expected, if $\hbar\omega_0 = 0.1$ eV is assumed as a representative phonon energy. As seen in the last column of table 3, for the free polarons the value 0.13 eV is rather close to this predicted one. For the bound polaron the experimental value is lower, since the peak energy M is additionally caused by the shift E_C of the initial level due to the defect potential: $M = 2E'_P + E_C$. The width, on the other hand, is only determined by the coupling to the lattice, E'_P ($W = \sqrt{\ln(2)4E'_P\hbar\omega_0}$). Although the lower values for W^2/M determined for the bound polarons P (i.e. Nb^{4+}_{Li}) and $Fe_{Li^{2+}}$, 0.09 eV and 0.07 eV, resp., indicate the influence of the stabilizing E_C, they still show that the optical absorption of these objects is mainly of polaron character (see equation (2.11)). Also this observation justifies considering them as bound polarons.

In order to point out the significance of the ratio W^2/M, it is mentioned that this ratio is much smaller for a typical colour centre. As an example, one finds for the absorption of the F-centre in KBr at 20 K $W^2/M \sim 3$ meV [79]. There the energy of the absorption peak is dominated by the electronic excitation between levels caused by the defect Coulomb field and not by the coupling to the lattice.

Now the various further values listed in table 3 will be discussed, first for the free polaron F, then for the bound ones, P and Fe^{2+}_{Li}. For the free polarons F the peak energy is $M = 2E_P$, leading directly to $E_P = 0.54$ eV (column 5 of table 3). From this, using the estimated $\hbar\omega_0 = 0.1$ eV, one calculates the width $W_{theo} = 0.39$ eV, almost identical with the observed one, $W = 0.37$ eV. Thus there is no extra stabilizing influence E_C, supporting the assignment of the absorption band peaked near 1 eV to free small polarons. An additional proof for this attribution comes from the measured activation energy, E_a, for the hopping transport of F : $E_a = (0.29 \pm 0.03)$ eV in Zn-doped and (0.24 ± 0.03) eV in Mg-doped reduced LN [50]. Within the limits of error these values are identical to the predicted one (equation (2.22)), $E_P/2 = 0.27$ eV.

Equation (2.23), expected for the adiabatic situation $J > \hbar\omega_0$, predicts a lower activation energy. Apparently the nonadiabatic case applies. The activation energy for hopping, $E_a = E_P/2 \sim 0.27$ eV is then also the activation energy of polaron mobility. In section 5.1 it will be shown why the previously reported value, $E_\mu = 0.42$ eV [80], is so different from the present experimental result and how this discrepancy can be removed by a reinterpretation of Nagels' thermopower data on the basis of the bipolaron model.

In the present context we also point out that the peak energy 0.94 eV (peak parameter $M = 1.09$ eV) of the free polarons in LN is rather high, if compared with those of polarons in other oxide materials, e.g. $BaTiO_3$ (0.6 eV) [81] or TiO_2 (0.7 eV) [37]. This indicates that the coupling of free electrons to the LN lattice is extraordinarily strong. From the model for F in figure 3.2 one expects a coupling of an extra electron in the orbital shown to an axial displacement, also partly responsible for the ferroelectricity of LN. The softness of the corresponding vibration mode may be the cause of the strong coupling to the lattice.

Now the values of E_P, E'_P and E_C related to F, P and Fe_{Li}, which are determined from the directly accessible M and W via the relations $M = 2E'_P + E_C$ and $W^2 = \ln(2)4E'_P\hbar\omega_0$ (cf table 3), are discussed. According to table 3, the derived data fulfil the expected trends: along the sequence F, P, and Fe_{Li} the peak energies M rise, and this is caused by the increase of the values E'_P and E_C. Both are larger for the bound polarons than for the free one, F.

For the bound polarons P the polaron energy, $E'_P = 0.58$ eV (table 3), is derived from the width W. As expected, this is larger than the polaron energy E_P of F, because of the enhanced stabilizing distortion, caused by defect prelocalization. From the peak position M the value E_C can then be derived: $M = 2E'_P + E_C$, yielding $E_C = 0.55$ eV. These values are comparable to those reported by Herth *et al* [82] for this system: $E'_P = 0.66$ eV and $E_C = 0.4$ eV. Regarding this comparison it should be noted that we had reason to fit only the low energy absorption data up to the peak maximum, as motivated above and discussed in section 4, whereas Herth *et al* [82] also took into account their absorption data at energies above the band maximum in the fitting.

Also the defect charge state Fe^{2+}_{Li} can be considered to be a small polaron, here bound to the defect core Fe^{3+}_{Li}. Analysing the data in table 3 in a way analogous to P, the related entries in table 3 are determined. The polaron energy $E'_P = 0.70$ eV is still larger than for P. The responsible stronger prelocalization by the defect attraction is also expressed by the larger value of $E_C = 1.22$ eV. Comparing the values E'_P and E_C for $P(Nb^{4+}_{Li})$ and Fe^{2+}_{Li}, it can be deduced that the Coulomb prelocalization is stronger for Fe^{2+}_{Li}, leading to a larger value for E_C and, accordingly, also for E'_P.

Next the parameters derived from the absorption band of the bipolarons will be treated. Here the value of E_C cannot be determined separately from the Coulomb repulsion U. From the values for M and W only the difference $E_C - U = 0.30$ eV (table 4) is available. That part of M which is caused by lattice distortion can thus be calculated: $M - (E_C - U) = 4E'_P$. Using this corrected value instead of the peak parameter M in W^2/M, one finds $W^2/(M-(E_C-U)) = W^2/4E'_P = 0.13$ eV, which is the target value expected for small polarons, if only influences caused by coupling to the lattice are included. Hence, the relation between shape and peak position of the absorption of B also supports the assignment to bipolarons. We continue by discussing the information conveyed by the parameter of the binding energy, ε_b. Table 1 shows that this can be related to the peak energy, M, by $\varepsilon_b = M - 2E_{Pstab}$. Here $2E_{Pstab}$ is the stabilization energy of two dissociated electrons, forming two bound polarons P. For the actual LN situation, two such separated polarons P are the next stable alternative to both electrons being paired as the bipolaron B. It is thus the sum of their ground state stabilization energies, $2E_{Pstab}$, which have to be subtracted from the total energy of two electrons in B, in order to arrive at the binding energy of B. As discussed before, the stabilization is the sum of that induced by distortion plus that caused by the defect energy E_C. From the entries in table 3, line 3, one calculates $E_{Pstab}(P) = 0.58\,\text{eV} + 0.53\,\text{eV} = 1.11$ eV. Using the observed bipolaron peak energy parameter, $M = 2.5$ eV, one thus expects the bipolaron binding energy to be $M - 2E_{Pstab} = 0.28$ eV. This compares very favourably with the observed one, $\varepsilon_b = 0.27$ eV. A similar value for the bipolaron binding energy has also been found for such a system in boron carbide [29]: $\varepsilon_b = 0.20$ eV had been determined by monitoring the thermal dissociation using high temperature EPR measurements.

The width of the bipolaron absorption band is predicted to be larger than that of a single polaron. For a one-site bipolaron, an increase by a factor of $\sqrt{2}$ is expected (section 2.3), if the related E_P are identical. We assume that, approximately, this one-site model is also applicable to the present situation, because for a bound bipolaron the two electrons will tend to be concentrated near $Nb^{4\bullet}_{Li}$, i.e. near the more attracting one among both ions in the bipolaron. This is borne out by the recent first-principles simulation of the electron densities in the bipolarons [74]. From the relevant entries in tables 3 and 4 it is seen, indeed, that the width of B is correspondingly larger. The polaron energies E'_P of P (0.58 eV, second line, second column of table 3) and E'_P of B (0.55 eV, third column of table 4) are nearly identical. Under this condition the width of B (0.55 eV, table 4) is expected to be larger by a factor of $\sqrt{2}$ than that of P (0.40 eV, table 3). This is fulfilled indeed: $0.55\,\text{eV} \approx \sqrt{2} \times 0.40\,\text{eV}$.

In particular, this fact but also the further observations on the peak energies, the widths and the binding energies of the optical absorption bands treated in this section are fully consistent with the polaron/bipolaron model.

It is conceivable that electron pairs bound to *extrinsic* defects can also be stabilized by joint lattice distortion, possibly leading to extrinsic bipolarons. Investigations by Corradi *et al* [83] point to the possible existence of Ti^{3+}_{Li}–Nb^{4+}_{Nb} and Ti^{3+}_{Li}–Ti^{3+}_{Nb} bipolarons in Ti-doped LN.

A remark is appropriate concerning the fact that the intensities of the treated absorption bands are only weakly dependent on light polarization. This appears to be in conflict with the polaron ground states, well aligned along the crystal axis, as shown in figure 3.2. Since, however, the optical transitions are of the charge transfer type, connecting the

Table 5. Comparison of the peak energies (in eV) of the various polaron types in LT and LN.

	LT	Ref.	LN	Ref.
Free polaron F	0.79	[84]	0.94	[50]
Bound polaron P	2.11	[85]	1.64	[77]
Bound bipolaron B	2.68	[85]	2.50	[75]

initial polaron site with each of the equivalent neighbour sites, where the polarization is roughly given by the corresponding transfer direction, it is plausible that the superposition of all these transitions is essentially unpolarized. Only intra-polaron transitions, related to local excitations at the respective sites, would be expected to have sharp polarization dependences. These intra-d polaron absorptions, however, are expected to be rather weak. This is discussed in more detail at the end of section 4.

Also reduced or optically excited $LiTaO_3$ (LT) exhibits absorption phenomena which can be attributed to the polaron types F, P and B [84, 85]. The peak energies are somewhat shifted with respect to those of their counterparts in LN, see table 5. It is remarkable that the peak energy of F (LT), 0.79 eV, is lower than that of F (LN), 0.94 eV. Since the peak energies for free polarons are only determined by the related polaron energies, this means that the coupling of a free electron to the LT lattice is weaker than in an LN crystal. The peak energies of the bound polaron objects in LT, P and B, on the other hand, are higher than in LN. This might point to the fact that the defect binding energies, E_C, are somewhat larger for LT than for LN. A definite answer can only be found if both parameters E_C and E'_P can be determined separately. The experimental information available at present on the bands in LT is not sufficient, however, to infer the polaron energies E_P (and E'_P) from the respective band widths. Although they behave similarly to those in LN, rising with the related peak energies, the low energy slopes especially of F and P are a little steeper than expected for ideal small polarons, preventing a reliable evaluation of E'_P on the basis of small polaron theory. It cannot be excluded that the polarons in LT tend to behave like those of intermediate size. The smaller coupling to the lattice might indicate this.

4. Refined treatment of the optical absorption of small polarons

4.1. Optical absorption of small polarons including final site tunnelling

Figure 3.8 shows the absorption band of the free polarons F in LN. Only the low energy onset of this band is reproduced by the corresponding theory (equation (2.9)). Such deviations between predicted and high energy parts of small polaron absorptions have been reported often, see e.g. [25].

The shape of the predicted optical absorption of free small polarons (equation (2.9)) is based on the assumption that the absorbed photon transfers the trapped electron from the ground state orbital at the initial site to an analogous ground state orbital at one equivalent final site (figure 2.1). This approach

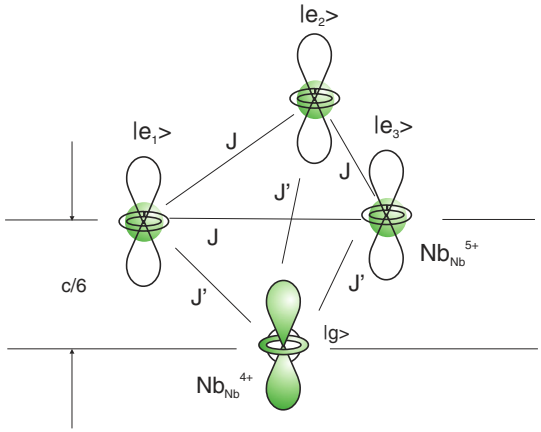

Figure 4.1. Three nearest Nb^{5+}_{Nb} ions surrounding a Nb^{4+}_{Nb} free small polaron having the orbital ground state $|g\rangle$. The neighbours are situated in a plane at $c/6$ above the plane of the polaron. There are six further equivalent Nb^{5+}_{Nb} ions in the plane of the Nb^{4+}_{Nb} polaron (at $c = 0$), hexagonally centred around it, and three further ones (not shown either) at $-c/6$. At the three final sites, which are indicated in the figure, equivalent 4d $(3z^2–r^2)$ type empty orbitals, $|e_i\rangle$, are shown. The labels J and J' symbolize the transfer integrals between the respective sites. Their values are symmetry related, as marked.

apparently fails to reproduce the high energy tail of a small polaron absorption. In a qualitative way it is discussed in the following how a solution to this problem can be found. We start by considering that there is not only one neighbour ion equivalent to the initial polaron site but several of them, which are related to each other by symmetry as determined by the crystal structure, see figure 4.1. The most simple systems involving such a set of equivalent final sites are represented by O^- hole small polarons, self-trapped with a polaron energy of typically 1 eV at one of the O^{2-} ions forming the inner surface next to a cation vacancy in oxide materials [13]. An O^- hole polaron bound to the Li vacancy in LN is a special example found in this category [13]. Light-induced polaron transitions occur between O^- and the equivalent O^{2-} ions on the inner surface. Such O^- hole polarons and their orbital structure have been studied in detail, using electron paramagnetic resonance and optical methods. On this reliable basis compelling evidence has been identified that the hole, transferred optically from its initial trapping site to one of its equivalent final site neighbours, will tunnel among all the final sites, which are symmetrically related in the distorted geometry caused by the polaron localization, before the lattice relaxes to retrap the hole at one site. This tunnelling leads to excited state splittings, typically by 0.4 eV [13], creating a density of final states spreading over a wider energy range than if optical transitions to only one neighbour ion are considered.

Figure 4.1 visualizes how this established situation can be transferred to the case of a Nb^{4+}_{Nb} small polaron in LN, together with three of its Nb_{Nb} next neighbours. At the initial site the electron populates the orbital $|g\rangle$, of 4d $(3z^2–r^2)$ type, as generalized from figure 3.2. Such orbitals are stabilized locally as the ground states by the crystal field. The distortion of the surrounding lattice, not shown, mediates the formation of a small polaron, which is free in the present case (figure 4.1),

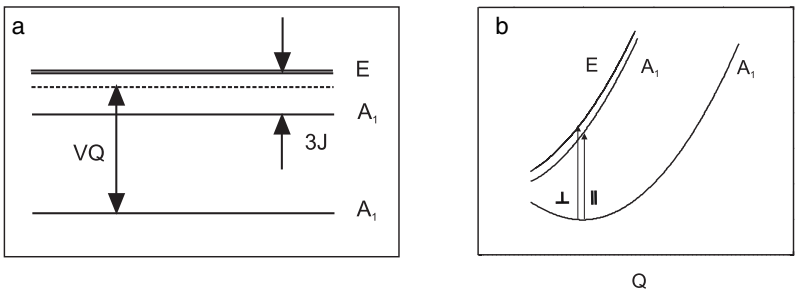

Figure 4.2. Visualization of optical polaron transitions from an initial site orbital ground state (see figure 4.1) to excited states resulting from tunnelling of an optically transferred carrier among all the equivalent neighbours. For simplicity, only three of the twelve equivalent Nb_{Nb} ions next to the initial Nb_{Nb}^{4+} polaron are included in the introductory approach. (a) Only the tunnelling levels depending on J and the coupling to the lattice, linear in Q, are included. (b) In addition the elastic energy of the lattice, quadratic in Q, is considered schematically. The polarization of the transitions, taking place under Franck–Condon conditions, is given by the symmetries of the orbitals, as indicated (assuming C_{3v} symmetry). The mentioned circumstances are seen to lead to a superposition of two Gaussian-like bands, with the indicated polarizations. It is seen that tunnelling among the final states leads to additional density of states at higher energies. Since in the actual LN crystal there are not three but twelve equivalent neighbours, a superposition of a correspondingly higher number of tunnelling orbitals will determine the optical properties. Still, their intensities can depend slightly on polarization.

Table 6. The transfer integrals coupling the various site orbitals sketched in figure 4.1.

	$\|g\rangle$	$\|e_1\rangle$	$\|e_2\rangle$	$\|e_3\rangle$
$\langle g\|$	$-VQ$	J'	J'	J'
$\langle e_1\|$	J'	0	J	J
$\langle e_2\|$	J'	J	0	J
$\langle e_3\|$	J'	J	J	0

because only Nb_{Nb} ions are involved. The equivalent orbitals at these potential final sites, $|e_i\rangle$, are symbolized by equal density contours. These states, as sketched, are typical for conduction band states near a defect, in the present case near a lattice perturbation caused by a small polaron.

The arrangement shown in figure 4.1 is a simplification of the actual cation environment of the Nb_{Nb} ions in LN, where each Nb lattice ion is surrounded by twelve equivalent neighbours of this type. This simplified scheme allows us to outline the essentials of the argument as applied to LN. The deviations from this simple model in an actual LN crystal and their influence on the excited state density of states will be discussed below.

The following topological matrix (table 6) is a generalization of the Hamiltonian in equation (2.8), as adapted to the situation of figure 4.2. It is spanned by the orbitals shown occurring in the selected cluster.

Here $-VQ$ is the lowering of the energy of the electron at the initial site caused by the polaron lattice distortion (figure 2.2); the quantities J' and J indicate the two expected types of transfer integrals between the orbitals, figure 4.1. For a fixed value of Q the eigenvalues of the Hamiltonian are shown in figures 4.2(a) and (b). Also the expected electron transitions, corresponding to the peak energies of the polaron absorption bands, and their polarizations are shown. It is seen that the tunnelling of the excited electron causes a spread of the final density of states reached by charge transfer transitions from the initial site. The polarization of the transitions is seen to depend on the transition energy, as indicated in figure 4.2(a). For the initial simplified situation two approximately Gaussian bands are expected, clearly representing an absorption band tail spreading over an extended energy range. The band shifts caused by excited state tunnelling are not taken into account quantitatively in tables 3 and 4. Corresponding corrections of the level energies in the given complicated settings probably have to wait for a treatment with reliable quantum-chemical methods.

As mentioned above, the real arrangement of neighbouring Nb_{Nb} ions around a given Nb_{Nb} ion in LN is more involved: there is a total of twelve next Nb_{Nb} neighbours around each Nb_{Nb} site; six of them form a hexagonal pattern coplanar with and centred around the initial Nb_{Nb} polaron site (at $c = 0$); three further Nb_{Nb} neighbours are arranged (as shown in figure 4.1) in a plane at $c/6$ above this plane and three Nb_{Nb} at $-c/6$. After an optical excitation of the electron to any of these surrounding Nb_{Nb} ions more tunnelling paths are open than in figure 4.1. This will lead to a modification of the excited state density as compared to that corresponding to figure 4.2: four times as many states are present in the energy range of the excited states shown there. Therefore, it is unlikely that the individual bands caused by this superposition can be resolved experimentally. This is in contrast to the situation of some of the O^- bound hole polarons in oxide materials [13], mentioned here as models for the present problem; there the configuration can be simple enough to resolve the excited state splittings and their polarizations.

Since, however, the total symmetry of the Nb_{Nb} arrangement is threefold axially symmetric, there will only be two types of representations, A_1 and E (assuming C_{3v} symmetry), characterizing the tunnelling states derived from the orbitals in figure 4.1. These can be reached from the polaron ground state, A_1, by light being polarized parallel and perpendicular to the c axis, resp. The superposition of the densely spaced optical bands can thus show some dependence on the optical polarization. The small polaron absorption bands of P and B shown in section 3 tend to be somewhat stronger for σ-than for π-polarization. Therefore transitions to states of E type from the A_1 ground state dominate those to A_1 type final states. For the F polarons the opposite tendency prevails.

Because tunnelling competes with the formation of small polarons, too large tunnelling splittings could argue against the presence of small polarons. Usually the properties of small polarons are evaluated under the condition $J \ll E_P$, not leading to high energy tails of the absorption bands (see, e.g., [14, 15]). This condition is somewhat relaxed in [19]. In discussing the reasons for larger J values, which are still consistent with the presence of small polarons, we point out the following arguments. (1) Crystals investigated experimentally are not ideal and charge carriers will be biased for localization at one site by weak lattice irregularities. This will support the formation of small polarons even in the presence of sizeable transfer integrals J. In Li-deficient LN this is expected to be caused by the high density of intrinsic defects. (2) The excited state splittings are characterized by transfer integrals valid in the distorted environment corresponding to the small polaron formed, J_{dist}. They can be larger than the rigid lattice transfer J competing with the polaron formation. (3) With the well-characterized O^- bound hole systems [13] it has been demonstrated that large excited state splittings do not contradict small polaron formation necessarily.

As judged by the high energy deviations between prediction and experiment, the same arguments forwarded so far to explain the high energy absorption tails of the free small polarons, F, appear to apply also for bound small polaron absorptions $P(Nb_{Li}^{4+})$ (figure 3.6) and of the bipolarons B (Nb_{Li}^{4+}–Nb_{Nb}^{4+}) (figure 3.5), etc. Reyher *et al* [76] previously have introduced tunnelling among equivalent final states to describe the details of the optically detected magnetic resonance (ODMR) of Nb_{Li}^{4+} (P).

High energy tails of polaron absorption bands are well known for large polarons [20]. They originate from transitions from the polaron ground state level to the conduction band states, in a similar way as outlined here for small polarons. Therefore small polaron transitions with wide high energy tails could be mistaken for large polarons. It is because of this reason that Kitaeva *et al* [86] ascribed the free polaron, F, absorption in LN to large polarons. The F polarons, however, are characterized by hopping transport [50], definitely inconsistent with large polarons. As demonstrated before in this section, wide high energy absorption band tails can also be a property of small polarons.

So far only optical transitions from the initial orbital ground state to the equivalent ground state orbitals at the final states have been considered, i.e. to those of the type shown in figure 4.1. Still following the paradigmatic cases of the bound O^- hole polarons [13], it can be expected that also transitions to excited state orbitals at the final sites can occur, if the selection rules permit. This will further add to the spreading of the small polaron absorptions to higher energies than predicted so far.

For the case of the free polaron F, as an example, the orbital level structure given by figure 4.3 is valid at each of the sites involved, see, e.g., figure 4.1. The initial ground state, $|g\rangle$ in figure 4.2, corresponds to the $^2A_1$ lowest orbital in figure 4.3. It is expected that transfers not only to such $^2A_1$ at the neighbouring equivalent sites take place, but also to all crystal field excited orbital states there, which have finite overlap with the initial ground state, $|g\rangle$.

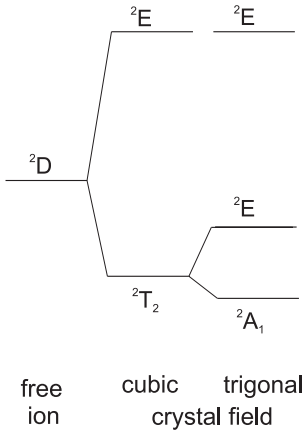

Figure 4.3. Orbital level scheme at the position of $|g\rangle$ and of each of the representative $|e_i\rangle$ orbitals in figure 4.2. It is expected that there will be finite transfer paths from the initial state $|g\rangle$, corresponding to the trigonal field ground state, $^2A_1$, to the various excited orbital states at the final equivalent sites, if the selection rules permit.

Of course, optical crystal field transitions implied by the level scheme in figure 4.3 can also occur at the initial site of the polaron. They would correspond to an intra-polaron transition, in contrast to the inter-polaron charge transfers, so far exclusively treated in this review. In the latter situation, the transfer mixture between the involved initial and final states give them an indefinite parity; the inter-polaron transitions are thus electric-dipole-allowed. Intra-polaron transitions taking place between crystal field states, dominantly having d-character, are essentially dipole-forbidden and thus have low intensity. These properties of intra- versus inter-polaron transitions are also documented by the O^- bound polarons treated in [13].

5. Dependence of polaron and bipolaron concentrations on temperature, light intensity and time

5.1. Concentrations as depending on temperature

We determine how the concentrations b, p and f (see section 3.2) of the three types of electron polarons in reduced congruent LN depend on temperature. Here we start with the consideration of (bound) polarons P and bipolarons B and introduce free polarons F later. Both P and B form at the Nb_{Li} sites in such crystals. The chemistry of P and B thus takes place on the Nb_{Li} subset of the Nb ions in LN, and all related statistical arguments have to take into account only the number of Nb_{Li} sites. This is also valid for the bipolarons B, since the Nb_{Li} partner of each B is uniquely related to only one fixed neighbour partner from the Nb_{Nb} lattice.

These bipolarons can be dissociated thermally into polarons according to the reaction $B \leftrightarrow P + P$. In more detail this should be written as $B + V \leftrightarrow P + P$, since unoccupied Nb_{Li} sites, labelled V, are consumed when occupied by an electron, forming P. In the following we shall relate all concentrations to the number of available Nb_{Li} sites. Then the concentration of vacant sites v, i.e. unoccupied Nb_{Li} defects

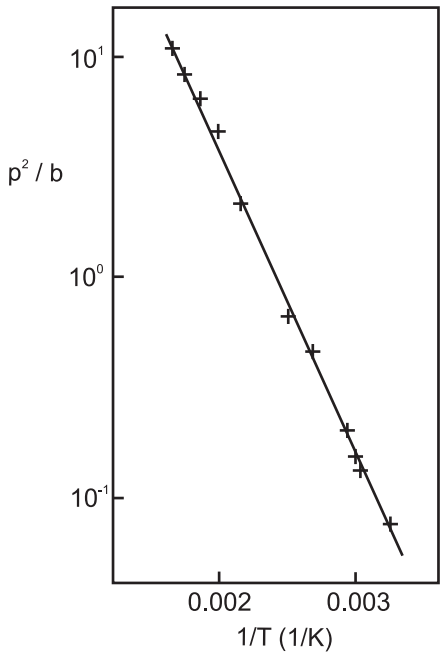

Figure 5.1. Dependence of the ratio $p(T)^2/b(T)$, determined from figure 3.4, on $1/T$ [75]. It is seen that this ratio fulfils $p(T)^2/b(T) \propto \exp(-\varepsilon_b(kT))$ (equation (5.1)) with $\varepsilon_b = (0.27 \pm 0.02)$ eV.

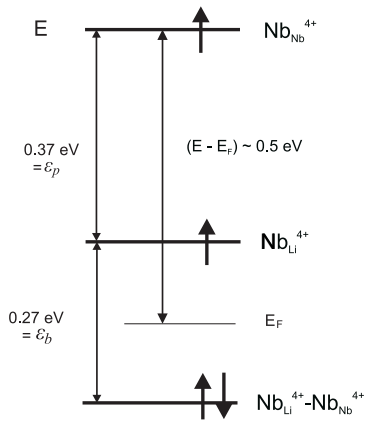

Figure 5.2. The energies determining the concentrations of B, P and F. As mentioned in the text, the creation of one single electron in P from paired ones in B needs an energy of $\varepsilon_b/2$. This fixes the position of the Fermi level as indicated. The value $(E - E_F)$ has been determined from thermopower studies, see text. The values ε_b and ε_p have been inferred from other experiments, also see text. In a second way they independently imply that excitations to the conduction band are activated from E_F by $(\varepsilon_b/2 + \varepsilon_p) \sim 0.5$ eV.

relative to the total number of Nb_{Li} sites, is given by $v = 1 - p - b$, since also B requires only one of the available Nb_{Li} sites. The temperature dependence of the concentrations b and p is governed by the corresponding law of mass action, with ε_b the bipolaron binding energy, i.e. the energy difference between two separated polarons P and two electrons bound together as a bipolaron B [75, 59]:

$$p(T)^2/b(T)v(T) = \exp(-\Delta F_b/kT) = \exp(\Delta S/k)\exp(-\varepsilon_b/kT) = g_p \exp(-\varepsilon_b/kT), \quad (5.1)$$

where $\Delta F_b = \varepsilon_b - T\Delta S$ is the change of the free energy accompanying the bipolaron dissociation, with ε_b the corresponding energy. For two separated single polarons, each having spin $S = 1/2$, the number of accessible states is four times higher than for the singlet bipolaron ground state. Therefore the entropy factor $\exp(\Delta S/k) = g_p$ in equation (5.1) is 4, implicitly contained in the derivation of the law of mass action for bipolarons by Emin [59]. The total concentration of electrons present either in the form of bipolarons or polarons is

$$c = 2b(T) + p(T). \quad (5.2)$$

It has been shown [87, 88] that the number of electrons supplied by a typical reduction process (oxygen partial pressure $p_{O_2} < 2 \times 10^{-8}$ bar, $T = 800\,^\circ$C, duration 6 h) is low compared to the available Nb_{Li} sites: $(P + B)/Nb_{Li}^{5+} < 10^{-2}$. This supports earlier conclusions by Smyth [10]. Therefore, the related concentrations fulfil $c \ll 1$ and $v(T) \approx 1$.

Plotting the ratio $p(T)^2/b(T)$ (deduced from the measurements given in figure 3.4) over $1/T$ (figure 5.2) leads to a bipolaron binding energy $\varepsilon_b = (0.27 \pm 0.02)$ eV on the basis of equation (5.1).

Using equations (5.1) and (5.2) one derives the temperature dependences $p(T)$ and $b(T)$:

$$p(T) = 1/4g_p n_b(-1 + \sqrt{1 + 2c/1/4g_p n_b}) \quad (5.3a)$$

$$b(T) = 1/2(c - p(T)) \quad (5.3b)$$

where $n_b = \exp(-\varepsilon_b/kT)$. This result (equation (5.3*a*)) is consistent with the general expressions for $p(T)$ derived by Emin [59], here specialized for $c \ll 1$.

Now it is taken into account that the electrons in the polarons P can be further excited to the conduction band, forming the free polarons F at Nb_{Nb} sites: $P \leftrightarrow F$. These tend to be recaptured, usually rather fast, at available empty Nb_{Li} antisite defects, then again forming P. They are thus the dominating single-electron species at low temperatures, to be specified below. Since the F polarons are situated in the sublattice of normal Nb sites (Nb_{Nb}), the number of available sites is larger by the factor $Nb_{Nb}/Nb_{Li} \approx 100$ for congruently melting LN. The concentrations $b(T)$, $p(T)$ and $f(T)$ now follow from the two laws of mass action:

$$p(T)^2/b(T)v(T) = g_p \exp(-\varepsilon_b/kT),\ g_p = 4 \quad (5.4)$$

$$f(T)/p(T) = g_f \exp(-\varepsilon_p/kT),\ g_f \approx 100. \quad (5.5)$$

Figure 5.1 visualizes the related energy levels. As mentioned, $\varepsilon_b = (0.27 \pm 0.02)$ eV [75] (figure 5.1); the value of ε_p has been determined to be $\varepsilon_p = (0.37 \pm 0.05)$ eV [29]. This is the difference in the activation energies of conductivity, measured in the dark and under an illumination dissociating all bipolarons. It will be shown below that the sum $(\varepsilon_b/2 + \varepsilon_p)$ can be identified independently also from a reinterpretation of previous measurements of the thermopower of reduced LN [80].

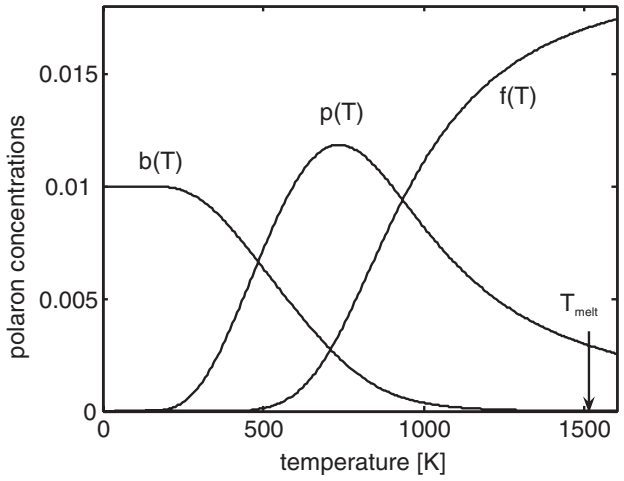

Figure 5.3. Concentrations $b(T)$, $p(T)$ and $f(T)$ in thermal equilibrium. The electron concentration c (per site), independent of temperature, was assumed to be 0.02. LN melts congruently at $T_{\text{melt}} = 1526$ K.

With these relations and $c = 2b(T) + p(T) + f(T)$ one can now solve for $b(T)$, $p(T)$ and $f(T)$. Since the number of electrons involved is not changed, again $c \ll 1$ and $v \approx 1$, and one derives

$$p(T) = 1/4 g_p n_m n_b \left(-1 + \sqrt{1 + 2c/(n_m^2 n_b)}\right) \qquad (5.6)$$

$$b(T) = 1/2(c - n_m p(T)) \qquad f(T) = g_f n_p p(T)$$

with $n_b = \exp(-\varepsilon_b/kT)$, $n_p = \exp(-\varepsilon_p/kT)$ and $n_m = 1 + g_f n_p$.

The temperature dependence of the concentrations, calculated with $\varepsilon_b = 0.27$ eV (3100 K) and $\varepsilon_p = 0.37$ eV (4320 K), are shown in figure 5.3, assuming a concentration $c = 0.02$ as an example.

It is seen that the dissociation of B starts already near 200 K. This is surprising in view of the dissociation energy ε_b, corresponding to 3100 K. The low temperature onset is caused by two circumstances: (1) the rise of entropy connected with the breaking of bipolarons (degeneracy 1) to two separated polarons (degeneracy 4) and (2) the fact that the increase of the concentration p is activated by $\varepsilon_b/2$, if a fixed initial concentration b_0 is assumed:

$$p \propto \sqrt{b_0/2}\exp(-1/2\varepsilon_b/kT). \qquad (5.7)$$

This means that the Fermi level, determining the excitation energy to the conduction band, can be taken to lie at $\varepsilon_b/2$ (see figure 5.1) [32]. Such a position of the Fermi level is typical for 'negative-U' systems [12].

It is an interesting consequence of equation (5.1) that $p/b \propto \sqrt{1/b}$, i.e. the larger the concentration of bipolarons the lower the relative concentration of polarons.

5.2. Temperature dependence of thermopower and DC electronic conductivity

Nagels [80] has performed an extended investigation of the electronic transport of reduced congruently melting undoped LN, including DC conductivity and thermopower. For the dependence of the thermopower α on temperature he found

$$\alpha_{\text{exp}} = -0.25V/T - 0.78 \text{ mV K}^{-1}. \qquad (5.8)$$

He interpreted this relation by assuming a single polaron ground state, using the expression $\alpha_{\text{th}} = -1/(qT)(E_F - AkT)$. It was not known then that the ground state of reduced LN is bipolaronic. Interpreted on the basis of only unpaired polarons ($q = 1e$), this equation means: an electron is thermally excited from the Fermi level E_F to the conducting state (at energy 0), where it can adapt to the applied temperature gradient. For the adjustment of a single carrier to this thermal situation, comparison of α_{exp} and α_{th} would imply that E_F lies 0.25 eV below the conduction band edge. If two carriers are excited simultaneously ($q = 2e$), the measured thermopower leads to a doubled E_F, 0.50 eV. This is expected to occur in the case of a bipolaron ground state, resulting from the sequential hopping of the partner electrons followed by their subsequent recombination to a bipolaron [59]. The value 0.50 eV for the thermopower is consistent with data determined from other experiments, figure 5.2. We are grateful to Emin for comments concerning this reinterpretation of Nagels' data.

In the conduction band of LN the conductivity is carried by free small polarons F, characterized by an activation energy $E_\mu = 0.27$ eV. This value is in line with the optical absorption data of F (section 3.3). We shall show now that it allows us to interpret the dependence of the electronic conductivity σ on temperature, when interpreted on the basis of a bipolaron ground state:

$$\sigma = n_0 \exp(-E_n/kT)\mu_0 \exp(-E_\mu/kT)/T^x. \qquad (5.9)$$

Here, $n_0 \exp(-E_n/kT)$ is the density of the conducting polarons F. Being bound, the mobility of P and B is too low to contribute decisively to the DC conductivity. The value $E_n = 0.5$ eV is the position of the Fermi level (figure 5.2), partly determined by the bipolaron situation. The exponent x influences the temperature dependence of a prefactor [49] specific for thermally activated hopping: $x = 1$ applies for adiabatic hopping ($J > \hbar\omega_0$) and $x = 3/2$ for the nonadiabatic case. In order to isolate the exponentials $\exp(-E_n/kT)\exp(-E_\mu/kT)$ in equation (5.9), Nagels plotted σT^x versus $1/T$ and found the slopes $E_\sigma = 0.74$ eV ($x = 3/2$) and 0.72 eV ($x = 1$), resp. [80]. This corresponds to $E_\sigma = E_n + E_\mu$, with $E_n = 0.5$ eV leading to $E_\mu = 0.24$ eV and 0.22 eV, resp. Both values are close to $E_\mu = 0.27$ inferred in the alternative way, see section 3.3. The value 0.24 eV fits somewhat better, supporting the occurrence of nonadiabatic hopping for the conducting polarons in LN, in line with the analogous result in section 3.3. Previously [80], Nagels had arrived at the value $E_\mu = 0.42$ eV first by fixing the position of the Fermi level at 0.25 eV, as discussed, and second by using only the slope of the raw data, i.e. of the measured σ, not correcting for the denominator $1/T^x$. The activation energy of this 'raw' σ is 0.67 eV, leading to $E_\mu = 0.42$ with $E_n = 0.25$ eV. Summing up our reinterpretation, it is seen that the electronic conductivity of reduced LN can now be well understood on the basis of the presented small polaron/small bipolaron model.

5.3. Concentrations as depending on temperature and constant illumination

In the following we treat again the simpler situation, that the formation of free polarons is neglected (see figures 5.3). This mainly applies to low temperatures ($T < 500$ K). The law of mass action (equation (5.1)) represents the stationary solution of the rate equations:

$$\mathrm{d}b/\mathrm{d}t = -\beta b + \gamma p^2 \tag{5.10}$$

$$\mathrm{d}p/\mathrm{d}t = 2\beta b - 2\gamma p^2 \tag{5.11}$$

where β is the thermal dissociation rate and γ the recombination rate. The factors of 2 in equation (5.8) arise because the concentration $c = 2b + p$ is constant. The rate of dissociation induced by temperature and illumination is described accordingly by

$$\mathrm{d}b/\mathrm{d}t = -(\beta + qI\Sigma)b + \gamma p^2 \tag{5.12}$$

$$\mathrm{d}p/\mathrm{d}t = 2(\beta + qI\Sigma)b - 2\gamma p^2 \tag{5.13}$$

with Σ the bipolaron optical absorption cross section, q the quantum efficiency for dissociation and I the light intensity. It should be noted that q rises strongly with energy [77, 73]: photons of 2 eV dissociate only about 10% of all present bipolarons, whereas at 3 eV the efficiency is about 90%. The law of mass action, now including the effect of a constant illumination, then is

$$p^2/b = (\beta + qI\Sigma)/\gamma. \tag{5.14}$$

The quotient β/γ describes the mass action for $I = 0$, i.e. the temperature dependence as given by equation (5.4). This part causes the dissociation to dominate at high temperatures, whereas even slight light intensities tend to lead to complete dissociation at low temperatures (figure 5.4). At intermediate temperatures recombination to B takes place, favoured by low light intensities.

In deriving this figure it was assumed that the carrier concentration, as related to the number of the available Nb_{Li} sites, is $c = 0.02$ (equation (5.2)). Thus the initial relative bipolaron concentration at low temperature and $I = 0$ is $b = 0.01$, leading to $p = 0.02$ under complete dissociation. In modelling the first part of the mass action law (equation (5.14)), the experimentally determined dissociation energy, 0.27 eV, was inserted: $\gamma/\beta = 4\exp(-0.27\ eV/kT)$ (equation (5.4)). Concerning the second, light-dependent part, the following procedure was employed: (a) the photon fluxes were normalized to 532 nm as the wavelength of representative photons, (b) the dissociation cross section $q\Sigma$ was taken to be 2×10^{-22} m^2 [73] at this wavelength and (c) the recombination parameter γ was inferred from [31]: $\gamma = \gamma_0 \exp(-0.27\ eV/kT)$, where fortuitously the same activation energy as for the dissociation and mobility appears, established by Jermann *et al* [31] for the temperature range 295–393 K. An extrapolation of this relation to all temperatures was used in figure 5.4. The parameter γ_0 was inferred as 1.7×10^{-23} m^3 s^{-1} from [87] and [88]. It is seen that at low temperatures all bipolarons tend to be dissociated completely, even under low intensities I.

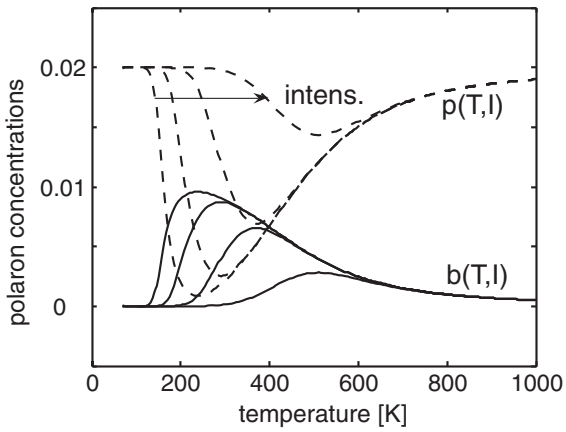

Figure 5.4. Dependence of the concentrations b and p (relative to the density of Nb_{Li} sites) on temperature and light intensity. At low temperatures even slight light intensities lead to complete dissociation. With rising temperature recombination to b occurs, before thermal dissociation dominates at high temperatures. The set of branches corresponds to the following intensities: 1, 10^2, 10^4, 10^6 W m^{-2}. The initial bipolaron concentration was assumed to be 0.01 (per Nb_{Li} site). This leads to a p concentration of 0.02 after dissociation.

5.4. Dynamic behaviour under switched cw illumination

Next we consider the time dependence of b and p in reduced LN, resulting from switching a constant illumination I on and off. Furthermore the change of the concentrations under varying intensity I will be described. Such investigations were performed experimentally by Jermann *et al* [31], yielding a rather direct further support of the polaron/bipolaron model. The concentrations p and b were determined by optical absorption measurements, employing weak probe light beams with energies near the peaks of the P and B absorption bands. For experimental reasons, the intensity of the dissociating light was kept so low that only rather weak light-induced deviations from the equilibrium concentrations were induced: $\Delta b_{li} \ll b$ and $\Delta p_{li} \ll p$. Equation (5.13) can then be written, assuming $\beta = 0$ and using the abbreviations $2q\Sigma b = \bar{g}$ and $2\gamma = r$:

$$\mathrm{d}p/\mathrm{d}t = \bar{g}I - rp^2. \tag{5.15}$$

The light-induced rise of p, following the application of an intensity I at $t = 0$, is calculated to be

$$\Delta p_{li}(t, I) = \Delta p^s_{li}(I) \tanh(\zeta_P \sqrt{I} t) \tag{5.16}$$

with

$$\Delta p^s_{li} = \xi_P \sqrt{I} \qquad \text{and} \qquad \xi_P = \sqrt{\bar{g}/r}, \qquad \zeta_P = \sqrt{\bar{g}r}. \tag{5.17}$$

Equation (5.16) indicates that the amplitudes of the light-induced polaron concentration changes as well as the speed of these changes vary as the square root of the intensity. After shutting off the illumination (at $t = 0$) the decay of the polaron concentration is expected to behave as

$$\Delta p_{li}(t, I) = \frac{1}{1/\Delta p^0_{li} + rt} \tag{5.18}$$

where $\Delta p_{\mathrm{li}}^{0}$ is the light-induced polaron concentration change at $t = 0$. Because the concentration $c = 2b + p$ is constant (f is neglected at low temperatures), complementary changes of b are expected and found.

These predictions were seen to be fully obeyed by the observed time dependences [31]. By fitting the experimental data to the observed dependences, the values for the parameters ξ_P, ζ_P and r could be determined. Equation (5.17) predicts: $K_{\mathrm{theo}} = \frac{\xi_P r}{\zeta_P} = \frac{\sqrt{g/r}}{\sqrt{gr}} r = 1$. The experimental data lead to $K_{\mathrm{exp}} = 0.9 \pm 0.2$. These observations of the dynamic behaviour under changing illumination thus support the polaron/bipolaron model.

5.5. Production of polarons under short laser pulses and their recombination

Recently, intense short light pulses ($\lambda = 532$ nm, $I_P^{\max} = 670$ GW m^{-2}, $t_P = 8$ ns) [90] have been used to dissociate bipolarons in reduced congruent LN and to investigate the time dependence of the subsequent backreaction of the created polarons to bipolarons. For such high intensities the analytical solutions presented in the previous section (section 5.3) under the condition $\Delta b_{\mathrm{li}} \ll b$ and $\Delta p_{\mathrm{li}} \ll p$ are not valid any more. In fact, strong decreases of the concentrations b and concomitant increases of p were observed to occur within the duration of the laser pulses. The decay of the concentration $p(t)$ to the initial situation, characterized by the recombination of the light-induced dissociation products P to the bipolarons B, was found to proceed by a stretched exponential, $p(t) = p(0)\exp(-t/\tau)^{\beta}$, with typically $\tau \approx 3$ ms and $\beta = 0.4$. For lower light intensities, $I_P < 100$ GW cm^{-2}, the decay had to be described by the superposition of two stretched exponentials, one characterized by short recombination times, $\tau \approx 1$ μs, the other one by longer ones, $\tau \approx 2$ ms. Measurements at different temperatures revealed that the recombinations are thermally activated by two distinct energies: $E_{\mathrm{slow}} = (0.52 \pm 0.05)$ eV and $E_{\mathrm{fast}} = (0.23 \pm 0.05)$ eV, resp. With increasing pulse intensity the second, slow component starts to dominate the decay behaviour.

So far a microscopic model is lacking which could explain the relevant recombination phenomena quantitatively. Stretched exponential decays, see also [90, 82, 91], usually result from a superposition of processes having various recombination times. Qualitatively, one has to start with the initial situation present after the exciting light pulse has ended: it is characterized by a distribution of B, P and F polarons. On the basis of their small polaron character, it is certain that the elementary steps leading to recombination consist in thermally induced hops to neighbouring sites until, eventually, bipolarons B are reformed. The hopping from F to a neighbouring $\mathrm{Nb}_{\mathrm{Nb}}^{5+}$ ion is expected to have the fastest rate, because the lacking defect potential ($E_C = 0$) leads to the lowest activation energies. If in such a process the electron is trapped at $\mathrm{Nb}_{\mathrm{Nb}}^{4+}$ axially neighbouring a bound polaron P, a bipolaron B is created again. Intermediate steps leading to this final situation consist in transfers from F to isolated $\mathrm{Nb}_{\mathrm{Li}}^{5+}$, forming P, from where thermally induced transfers occur slower, because the antisite defect potential, $E_C \neq 0$, causes a higher activation energy. After reexcitation the electron will also recombine finally to form B.

The influence of the pulse intensity on the decay kinetics can be assigned to the following scenario: at low intensities, an electron optically separated from B will end in close proximity to its initial position [92], because optical transfers occur to next neighbours with the highest probability. From there the backreaction, forming B at the initial site, will be fast. The higher photon density contained in high-intensity pulses raises the probability that charge carriers are reexcited to ions farther away from the initial site B before the backreaction occurs. Therefore, the majority of the dissociated electrons form intermediate concentrations of bound polarons P, from where the backreaction to B is slower. High intensities will thus cause a predominance of the slow recombination process, characterized by higher activation energies, as observed.

6. Discussion of alternative models for absorption changes caused in undoped $LiNbO_3$ by a raised Fermi level

In the previous sections it was shown that the reduction-induced optical absorption changes of congruently melting LN can be explained consistently on the basis of the presented 'small polaron/small bipolaron' model. Earlier, however, in some cases the related absorption features were interpreted by different approaches. In the following we shall compare and discuss the presented alternative models. They can be classified into the following categories: (A) different polaron-related models and (B) oxygen vacancy-related models.

We first list the relevant papers and then discuss and compare them in detail. Category A includes the investigations by Jhans *et al* [93] as well as Dhar *et al* [94], who interpret the optical absorption of as-reduced congruent material by single polarons. Akhmadullin *et al* [95] ascribe an absorption band with peak at 3.5 eV to pairs of bipolarons, so-called quadpolarons (q-polarons).

In category B, articles by Halliburton [77], Arizmendi *et al* [96], Hodgson *et al* [97], Garcia *et al* [97], Bredikhin *et al* [68] as well as Sugak *et al* [99] will be discussed. Furthermore a remark on the relation between small polaron optical absorption in reduced LN and luminescence observed with such systems by Zhang *et al* [100] is added.

6.1. Polaron-related alternative models

6.1.1. Optical absorption in terms of single small polarons. Jhans *et al* [93] presented a detailed discussion of conceivable models to explain the 2.5 eV band (attributed to bipolarons B before) and came to the conclusion that the adoption of a model involving small polarons is favoured, especially because several findings argue against oxygen vacancies as the cause of the absorption. They focused on single polarons because the theoretical treatment of only their optical properties was known at that time. This assignment was forwarded irrespective of the previously published proof [77] that as-reduced LN has a diamagnetic ground state. The authors remarked, however, that

they could not adequately reproduce the observed band by the established theory for single small polarons [15].

For the polaron model to be valid, they concluded that the related polarons must have a 'complex structure' in order to be consistent with the absence of a correlated EPR signal and to remove the lack of coincidence with Reik's small polaron predictions [15]. This postulated complex structure was shortly afterwards identified in the bipolaron model [101].

Irrespective of the same limitations Dhar and Mansingh [94] also proposed to base the 2.5 eV absorption on isolated small polarons.

6.1.2. Quadpolarons (q-polarons). After the introduction of the bipolaron model [2, 101] Akhmadullin *et al* [94] generalized this concept to account for another band appearing in reduced congruent LN after a low degree of reduction. This band is peaked at $E_{\text{peak}} = 3.5$ eV and has a half-width of about 0.4 eV (HWHM) (figure 6.1) [95]. The authors proposed that it is caused by the association of two bipolarons, cooperating to form a q-polaron (or quadpolaron) by distorting the lattice jointly. The intensity of the band decreases under illumination, especially for 3.65 eV light, covered by the discussed 3.5 eV absorption band. In this way an electron is transferred to a Nb_{Li} antisite defect, which is indicated by an increase of the responsible 1.6 eV band (figure 6.1). We shall show that the measured half-width, $\Delta W_{1/2,\text{exp}} \sim 0.4$ eV, is too low to be consistent with the lattice distortion required for a q-polaron to be stable. In order to have a total energy lower than that of its separated components the Coulomb repulsion among the involved four electrons must be overcompensated by a correspondingly strong stabilizing lattice distortion. Furthermore, in a q-polaron there is an extra repulsion among the carriers because of the Pauli principle: in a second pair of electrons, leading from a bipolaron to a q-polaron, the electrons cannot populate the same orbital ground state but must be promoted to a higher state, raising the total energy of the system [102]. Because the repulsion among four electrons is thus larger than between the two carriers in a bipolaron, the distortion stabilizing a q-polaron must be stronger than that of a bipolaron. This can be deduced by analogy to the argument demonstrating why a bipolaron can be stable, see section 2. Since a stronger lattice distortion necessarily causes a larger width of a related small polaron optical absorption band, it is expected that the optical features originating from a q-polaron are characterized by an optical bandwidth larger than that of a bipolaron.

For estimating a lower bound of the q-polaron linewidth, $\Delta W_{1/2,\text{est}}$, we can thus use the relevant expression for the bipolaron case (equations (2.16) and (2.18)):

$$\Delta W_{1/2,\text{est}} \sim \sqrt{2\ln(2)M(\hbar\omega_0)} = \sqrt{2\ln(2)(4E_{\text{P}} - U)(\hbar\omega_0)}. \tag{6.1}$$

In order to arrive at a lower bound for the expected linewidth, it is assumed that $U = 0$. Then the peak energy, 3.5 eV, would be totally determined by lattice distortion. Evaluating equation (6.1) under this condition, using $\hbar\omega_0 = 0.1$ eV, it is found that the value estimated on this basis, $\Delta W_{1/2,\text{est}} \approx 0.7$ eV, is larger already than the experimental

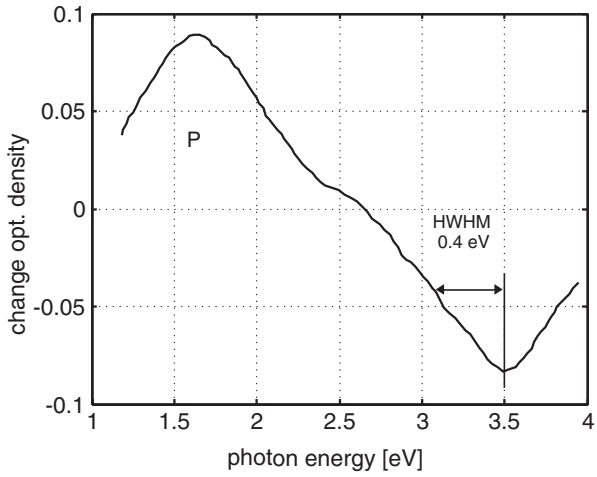

Figure 6.1. The 3.5 eV band mentioned in the present context decreases in favour for the 1.6 eV band, if the respective specimen is illuminated by 365 nm (3.4 eV) light, i.e. with an energy lying within the said band. This means electrons are excited from a corresponding low level, induced by an unknown defect, which causes the 3.5 eV band, to the conduction band. The excited electron is then captured at Nb_{Li}, responsible for the band at 1.6 eV. It is seen that the HWHM of the 3.5 eV band, 0.4 eV, is less than the 0.7 eV estimated as a lower bound for a q-polaron in LN. Adapted from [94].

width, $\Delta W_{1/2,\text{exp}} \approx 0.4$ eV. Since in reality the destabilizing influences, including the Coulomb repulsion U, not only among two but all four electrons, must be overcompensated by a correspondingly stronger distortion, a q-polaron should have a bandwidth wider than the estimated lower bound, 0.7 eV. It is thus seen that the observed bandwidth of the 3.5 eV band is incompatible with the q-polaron model. Seen differently, the comparatively low experimental bandwidth indicates that the peak energy is not caused by an excitation between energy levels determined only by lattice distortion. Rather, they must essentially be attributed to a rather deep defect potential, leading to a corresponding difference of the eigenstates of this potential. Some lattice distortion might also be present, but this is less decisive in determining the transition energy. At present no consistent model for the 3.5 eV band is seen. A further proposal for this band is dealt with in section 6.2.

6.2. Models involving oxygen vacancies

As has been summarized in section 3, Nb_{Li}^{5+} antisite defects and not oxygen vacancies, $V_O^{\bullet\bullet}$, are the majority intrinsic donors in congruently melting LN, compensating the cation vacancy acceptors, such as V'_{Li}. Smyth [10] has indicated that the chemical reduction of Li-deficient LN proceeds by the reaction

$$O_O + 2V'_{Li} + Nb_{Nb} \leftrightarrow 3/2O_2 + Nb_{Li}^{4\bullet} + 6e'. \tag{6.2}$$

This is a variant of the reaction listed in table 2, part c, where it is assumed that one oxygen ion, together with its two electrons, leaves the crystal in the form of Li_2O. Equation (6.2) demonstrates that also under reduction oxygen vacancies are not produced. Smyth [10] has furthermore shown that the

increase of the $Nb_{Li}^{4\bullet}$ concentration under reduction is small compared to their initial density in the as-grown, congruently melting material. The lacking permanent creation of oxygen vacancies in an oxide material under a reduction treatment appears to contradict common sense expectations. Therefore models involving oxygen vacancies as majority donors in LN have been forwarded repeatedly.

Such a model was also the basis for the interpretation of Halliburton's pioneering studies concerning the detection of the reduction-induced absorption bands, their modification by illumination and their correlation to EPR spectra [77]. As has been shown above, such bands can completely be ascribed to small polarons/bipolarons.

Oxygen vacancies were likewise postulated by Bredikhin *et al* [68] to explain the coloration of undoped congruently melting LN, induced not only by thermal reduction but also by electrical charge injection via solid state electrodes. Both methods have the effect to raise the Fermi level in the material. The absorption bands prepared by thermal reduction have been described above. Identical bands were observed after electrocoloration [68], implying that the same microscopic models should hold in both cases. The turnover of the band at 2.5 eV into the absorption at 1.6 eV, assigned to the process $B \rightarrow P + P$ before, under illumination and/or heating was not studied by these authors and therefore also not included in their discussion of the phenomena.

The electrocoloration performed by Bredikhin *et al* [68] proceeded by injection of oxygen ions or by extraction of Li ions under applied voltages at temperatures between 300 and 800 °C, using special solid state electrodes, which were blocking for electrons and permeable for the intended ions. The complementary electrons, necessary for charge compensation, were injected or extracted through counter electrodes, which were made from platinum, transparent for electrons and blocking for the ions. Also the reverse decoloration processes have been studied, occurring when the Fermi level is lowered under chemical oxidation or under electrical injection of oxygen ions or extraction of Li ions. This phenomenon has also been established by Falk *et al* [69], who proved that in this way the Fermi level can be lowered further than is possible by annealing in an oxygen atmosphere.

The authors also observed the band peaked at about 3.5 eV (figure 6.2), attributed to q-polarons by Akhmadullin [95], as discussed in the previous section (section 6.1). This band appears as the first one, when the Fermi level is raised from low values. With the Fermi level rising further, the band near 2.5 eV is then observed. The authors also investigated the time dependence of the coloration process under electrolysis, monitored by the speed with which the coloration fronts move through a specimen under an applied voltage. The related kinetic phenomena have been explained by the competition between the comparatively slow ionic and fast electronic diffusion. Similar phenomena, observed with the recharging of Fe_{Li}, have been reported recently and put into a wider context by Gronenborn *et al* [104].

Bredikhin *et al* [68] propose that the band at 3.5 eV is created when a preexisting empty oxygen vacancy, $V_O^{\bullet\bullet}$, captures one electron, leading to $V_O^{\bullet}$. On this basis they

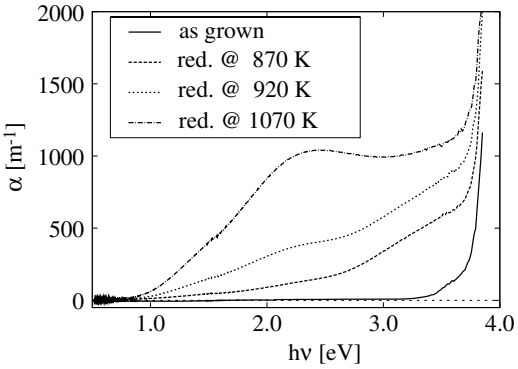

Figure 6.2. Steady state room temperature absorptions of selected nominally pure, congruently melting LN samples for various reduction temperatures [103]. Under weak reduction ($T = 870$ K) an absorption band peaked near 3.5 eV occurs. This has been treated in section 6.1. With rising temperature, corresponding to stronger reduction, the bipolaron band B (near 2.5 eV) appears.

then assume that the 2.5 eV band appears when a second electron is captured at $V_O^{\bullet}$, forming V_O^{x}. In addition to the oxygen vacancies, assumed to be present initially, further ones are also claimed to be created by oxygen extraction. As mentioned, the authors do not consider the nature of the band at 1.6 eV, resulting from the 2.5 eV band under heating or illumination. As a basis for their model they postulate that a LN crystal initially contains a sizeable concentration of empty $V_O^{\bullet\bullet}$, in its conventional congruently melting as-grown state. They estimate that a $V_O^{\bullet\bullet}$ concentration larger than 10^{19} cm^{-3}, equivalent to >530 ppm, is necessary to explain their findings based on the observations with the 3.5 eV band [68].

To our knowledge the investigation by Bredikhin *et al* [68] is the first one studying Fermi level changes in LN induced by electrical charge injection or extraction at elevated temperatures. Their investigation, however, only shows that LN in their experiments acts, depending on polarity, as a source or sink of oxygen atoms. Seen critically, they have no means in their experiments to decide what happens with the oxygen ions in the LN sample. Therefore they cannot exclude the reduction mechanism of LN, established earlier [10], see equation (6.2). As indicated in section 3, oxygen ions effusing from a specimen in a condition of low oxygen activity trigger the following subsequent ionic processes: uncompensated Li^{+} and Nb^{5+} ions are left back in the crystal, initially mainly near to its surface. The energy of the system decreases, if these ions diffuse into Li vacancies abundantly present in as-grown congruent LN, then forming Li_{Li}^{x} and $Nb_{Li}^{4\bullet}$. This ionic rearrangement is the consequence of the dissolution of entire $LiNbO_3$ molecules, still resulting in an intact oxygen sublattice and additionally filled Li vacancies. The decoloration under the addition of oxygen can be explained by the reverse movement of Li and Nb from the bulk of the crystal to the surface.

In discussing the scenario presented by Bredikhin *et al* [68], we start by emphasizing that the 2.5 eV band is caused by a 'negative-U' defect, as proved above. This property must be explained by all contenders for this defect, thus also by the $V_O^{\bullet}/V_O^{x}$ model [68]. The conditions appear to be favourable: the conceivable reaction $V_O^{x} \leftrightarrow V_O^{\bullet} + V_O^{\bullet}$ would signify the

dissociation and recombination of the two involved electrons. 'Negative U' means that V_O^x is the stable situation, where the repulsion U between the two electrons is overcompensated by joint lattice distortion and $V_O^\bullet$ is only metastable. We point out three observations which are in conflict with this model. First it is observed, in contrast to the expectation, that the band at 3.5 eV, attributed to $V_O^\bullet$ [68], is stable. No change of its intensity is observed after its production in the long run. Second, the peak energy of the claimed $V_O^\bullet$ is higher, 3.5 eV, than that of V_O^x, 2.5 eV. This is in conflict with the 'negative-U' property: the peak energies formally are: $M(2\text{-electrons}) = 4E_P - U + E_C$ and $M(1\text{-electron}) = 2E_P + E'_C$, where E_P is that part of the energy of the (first) electron which is caused by lattice distortion and E_C (or E'_C), the influence of the defect potential on the electron level energies. Experimentally, $M(2\text{-electrons}) < M(1\text{-electron})$ is found (2.5 eV < 3.5 eV). Assuming at first an absence of a defect potential ($E_C = 0$), this means: $4E_P - U < 2E_P$ or $2E_P - U < 0$, in contrast to the stability condition of a 'negative-U' system, $2E_P - U > 0$ (equation (2.14)). In order to still describe a stable two-electron situation, the related defect potentials would have to imply that $E_C - E''_C > 1$ eV. It is unlikely that the defect levels in an oxygen vacancy differ so much for one and two electrons. Third, since the linewidths of such systems are only determined by their lattice coupling, the width of the two-electron system (V_O^x) would have to be considerably wider than that of the one-electron system. This is not fulfilled experimentally: the widths are, resp., 0.55 eV as compared to 0.5 eV, i.e. they are nearly identical. These arguments, in addition to the defect chemistry of LN, unfavourable for the presence of oxygen vacancies in the material, oppose the suggested [68] assignment of the bands.

The responsibility of oxygen vacancies for the reduction-induced absorption bands in congruent LN has also been advocated in papers by Arizmendi *et al* [96, 105] and Garcia [98]. While for the band at 1.6 eV, the assignment to $Nb_{Li}^{3\bullet}$, i.e. to the bound small polaron P, is accepted by these authors, the band at 2.5 eV is again attributed to V_O^x, the oxygen vacancy containing two electrons. Previous arguments [32] against this assignment included the fact that chemical reduction of LN increases the density of LN [10], inconsistent with the formation of oxygen vacancies. The reduction process introduced by Smyth [10] (see section 3), not involving oxygen vacancies, on the other hand, correctly predicts such a density increase.

Hodgson *et al* [97] succeeded in also creating optical absorption bands near 2.5 eV (and in addition another one at 3.3 eV) by high energy electron irradiation of congruently melting LN. This phenomenon has a sharp threshold at electron energies corresponding to oxygen displacement in LN [96]. It is thus concluded that, under this treatment, oxygen vacancies are created in LN. This occurs in a metastable way: the absorption bands vanish by heating to 800 °C in vacuum. It is not clear whether the band at 3.3 eV is caused by a defect structure identical to or related to that causing the 3.5 eV band treated above [68, 95].

The main absorption band (near 2.5 eV) induced by e-irradiation has features identical to those described for the bipolaron band B. Supporting this, the transformation to the 1.6 eV band, attributed to P, is also observed when the temperature of the specimen is raised, identical to the phenomenon in figure 3.4, corresponding to thermal bipolaron dissociation. Lowering the temperature again, the 2.5 eV band is formed in a reversible way, identical to the prediction of the polaron/bipolaron model.

We cannot prove that no oxygen vacancies are created under the above threshold electron irradiation. Since, however, the resulting absorption bands are identical to those consistently ascribed to polarons and bipolarons in the sections above, we have to discuss how this assumption can be reconciled with the other observations. Since the energy level of $V_O^\bullet/V_O^{\bullet\bullet}$ is predicted to be more shallow, −0.16 eV, as predicted in [64, 106] than that of $Nb_{Li}^{4\bullet}/Nb_{Li}^{3\bullet}$ (−1.40 eV [64]) or the bipolarons (−1.66 eV [64]), it is expected that the V_O defects, possibly created, are emptied of their electrons immediately in favour of the antisite defects, forming bound polarons P or bipolarons B. Then only the optical spectra of the latter species are observed. According to this chain or argumentation they cannot be assigned to electron excitations at oxygen vacancies.

Finally, recently published investigations by Sugak *et al* [99] are discussed. These authors repeated *in situ* measurements of the optical absorption changes of reduced congruent LN; they monitored the transmission of a specimen held in an optical transmission cell passed by an atmosphere of 95%Ar + 5% H_2 at temperatures between RT and 800 °C. This reducing atmosphere could be exchanged quickly for oxygen. Apparently, it was not noticed by these authors that already earlier Koppitz *et al* [75] had performed measurements of the same *in situ* type, where the specimen was held in vacuum at temperatures between RT and 600 °C. It is thus not astonishing that Sugak *et al* [99] reported essentially the same results as those in figure 3.4 [75] for the low temperature range $T <$ 600 °C. The data in figure 3.4 have been shown above to be in full accordance with the polaron/bipolaron model. In spite of this Sugak *et al* [99] attribute the low energy band, near 1.6 eV, to hydrogen incorporated during their treatment, instead of the consistently established $Nb_{Li}^{3\bullet}$ defect, see above.

While the optical absorption changes in the low temperature range are completely reversible, at temperatures higher than about 600 °C irreversible alterations occur [99]. A new band peaked in the vicinity of 2 eV (16 000 cm^{-1}) [99] appears and this remains when the temperature is lowered in a constant atmosphere or when the sample is exposed to an oxidizing atmosphere. These findings share similarities with previous observations reported by Chan *et al* [107]: under conditions (equation (6.2)) reducing so strongly that all V'_{Li} in a crystal are consumed by the Li ions left over in the specimen during the reduction process, a new phase, characterized by Li_2O precipitations and separated from the LN host material, occurs. Sugak *et al* [99] attributed these changes to a loss of oxygen. No further arguments were presented.

6.3. Luminescence related to polarons

With LN, prepared in a way to exhibit the optical absorption of the bipolarons B, Zhang *et al* [100] have observed a rather

interesting luminescence phenomenon after excitation with visible light, consisting of two bands peaking at 1.48 eV and a weaker one at 1.30 eV [100]. So far an unambiguous assignment of this luminescence phenomenon is not given. We use the opportunity to mention that it is an intrinsic property of a small polaron that a (radiative) luminescence transition corresponding to the reverse of its optical absorption is not to be expected. The deexcitation of an absorptive small polaron transition rather proceeds by a radiationless multiphonon process. Bartram and Stoneham [108] have shown that it depends on the ratio Λ = excitation energy/relaxation energy whether luminescence is observed or not. Radiation will only occur for $\Lambda < 1/4$. For small polarons, however, $\Lambda = 1$, since following the Franck–Condon excitation the system relaxes all the way down to the initial energy by multiphonon emission (figure 2.5).

It is remarkable that a similar luminescence feature has been reported also for the parallel case of Fe_{Li}^{2+} in LN, having an orbital structure similar to Nb_{Li}^{4+}, by Parsons *et al* [109]. Also here a double band, with components peaked at 1.65 eV and a somewhat weaker one at 1.58 eV, has been identified. Parsons *et al* [109] stressed that the luminescence band cannot be explained by the reverse of the charge transfer optical absorption of Fe^{2+}. Also for this case an explanation of the phenomenon is still missing.

7. Summary

The scenario of intrinsic defects in LN is singular, as compared to that of the common oxide perovskites. The Li and Nb ions can exchange their sites rather easily; the most far-reaching consequence is the formation of $Nb_{Li}^{4\bullet}$ antisite defects. In the commonly used Li-deficient material, the Li substoichiometry is thus compensated by these intrinsic donors and not by oxygen vacancies, $V_O^{\bullet\bullet}$. The present review summarizes how the usually rather high concentration of $Nb_{Li}^{4\bullet}$ affects the electronic properties of the material. It is shown that electrons, made available by raising the Fermi level, are captured at $Nb_{Li}^{4\bullet}$, forming bound small polarons, $Nb_{Li}^{3\bullet}$ ($4d^1$). Pairs of nearest-neighbour Nb ions can trap two electrons, forming bound bipolarons: $Nb_{Li}^{3\bullet}(4d^1)$–$Nb_{Nb}^{4\bullet}(4d^1)$, representing the electronic crystal ground state. Avoiding the formation of antisite defects by doping with high concentrations of Mg, etc, allows us to study small polarons forming on the regular Nb sites of the material, $Nb_{Nb}^{4\bullet}$ ($4d^1$). Emphasis is on the investigation of the optical properties of these three manifestations of electron polarons. A general introduction to the theoretical features of small polarons and bipolarons, free as well as bound, in oxide materials, is given. Here a criterion is derived, based on the fact that for small polarons there is a fixed relation between width and peak energy of the absorption bands. This criterion is seen to be fulfilled for all the investigated absorption features. The absorption bands contain information on the defect-induced binding and on the coupling to the lattice. The latter is shown to increase with the defect potential, consistent with the nonlinear process of small polaron formation. For the bipolarons thermal and optical dissociation is studied. Discussing the dissociation energy, 0.27 eV, determined in this way, it is shown to be in accord with data determined for single polarons bound to the antisite defects. Qualitatively it is discussed why the absorption band for the present small polaron objects as well as those reported in the literature have high energy tails more intense than predicted by conventional small polaron theory. A section devoted to the dynamics of light-induced bipolaron dissociation and the recombination of dissociation products shows that all related phenomena can be explained on the basis of the existing concepts. The polaron/bipolaron model is thus found to be fully consistent with most of the reported investigations. This model is contrasted with other proposals involving only single free polarons or relying on the presence of oxygen vacancies, either present initially or created by chemical reduction. It is shown that in all these cases there are discrepancies with experimental facts. It is hoped that the present detailed review forms a reliable basis for the interpretation of related phenomena in the nonlinear optical applications of LN.

Acknowledgments

We are grateful to D Emin for discussions and correspondence concerning the treated polaron concepts. To D M Smyth we owe thanks for sharing his extended experience on the defect chemistry of $LiNbO_3$. H Donnerberg communicated useful advice on parts of the paper.

Appendix

Table A1. Overview on the nomenclature of the defects occurring in the text.

Nb_{Li}^{5+} ($4d^0$), $Nb_{Li}^{4\bullet}$	Antisite defect: niobium on Li site. The 5+ state of the isolated ion has an unfilled 4d shell above a krypton electronic configuration. It has a fourfold positive charge with respect to the replaced Li^+ ion. In Kröger–Vink notation [7] one positive relative charge is indicated by a • superscript; ‘marks one negative charge and x means zero relative charge
Nb_{Li}^{4+} ($4d^1$), $Nb_{Li}^{3\bullet}$	The antisite defect having captured one electron
$Nb_{Nb}{}^{5+}$ ($4d^0$), Nb_{Nb}^{x} Nb_{Nb}^{4+} ($4d^1$), Nb_{Nb}'	A ‘normal’ Nb ion of the lattice before and after having trapped one electron
Nb_{Li}–Nb_{Nb}	Preformed nearest-neighbour Nb pairs in LN containing one antisite defect
Nb_{Li}^{4+}–Nb_{Nb}^{4+} $Nb_{Li}^{3\bullet}$–Nb_{Nb}'	The pair has trapped two electrons. Then both have the configuration ($4d^1$)
Fe_{Li}^{2+} ($3d^6$), $Fe_{Li}^{\bullet}$ Ti_{Li}^{3+} ($3d^1$), $Ti_{Li}^{2\bullet}$ Mg_{Li}^{2+} ($3s^0$), $Mg^{\bullet}$	Analogous defect designations of extrinsic defects mentioned in the text
V_{Li}'	Li vacancy (Li^+ missing, therefore one negative relative charge)
$V_{Li}' - O^-$, $V_{Li}' - O^{\bullet}$	Li vacancy neighboured by a onefold positively charged oxygen ion (O^-)
$V_O^{\bullet\bullet}$, $V_O^{\bullet}$, V_O^{x}	Oxygen vacancies (one O^{2-} ion missing) with zero, one or two electrons

References

[1] Emin D 2007 Polarons *McGraw Hill Encyclopedia of Science and Technology* 10th edn, vol 14 (New York: McGraw-Hill) p 125
[2] Schirmer O F, Thiemann O and Wöhlecke M 1991 *J. Phys. Chem. Solids* **52** 185
[3] Arizmendi L 2004 *Phys. Status Solidi a* **201** 253
[4] Buse K, Imbrock J, Krätzig E and Peithmann K 2007 Photorefractive effects in $LiNbO_3$ and $LiTaO_3$ *Photorefractive Materials and Their Applications* vol 2, ed P Günter and J P Huignard (Berlin: Springer) p 83
[5] Hatano H, Liu Y and Kitamura K 2007 Growth and photorefractive properties of stoichiometric $LiNbO_3$ and $LiTaO_3$ *Photorefractive Materials and Their Applications* vol 2, ed P Günter and J P Huignard (Berlin: Springer) p 127
[6] Volk T and Wöhlecke M 2008 *Lithium Niobate–Defects, Photorefraction and Ferroelectric Switching* (Berlin: Springer)
[7] Kröger F A and Vink H J 1956 *Solid State Physics* vol 3, ed F Seitz and D Turnbull (New York: Academic) p 307
[8] Räuber A 1978 *Current Topics in Materials Science* vol 1, ed E Kaldis (Amsterdam: North-Holland) p 481
[9] Weis R S and Gaylord T K 1985 *Appl. Phys.* A **37** 191
[10] Smyth D M 1983 *Ferroelectrics* **50** 93
[11] Smyth D M 1986 *Proc. 6th IEEE Int. Symp. on the Applic. of Ferroelectrics* p 115
[12] Watkins G D 1984 *Festkörperprobleme* (*Advances in Solid State Physics* vol 24) p 163
[13] Schirmer O F 2006 *J. Phys.: Condens. Matter* **18** R667
[14] Reik H G 1963 *Solid State Commun.* **1** 67
[15] Reik H G and Heese D 1967 *J. Phys. Chem. Solids* **28** 581
[16] Eagles D M 1963 *Phys. Rev.* **130** 1381
[17] Klinger M I 1963 *Phys. Lett.* **7** 102
[18] Austin I G and Mott N F 1969 *Adv. Phys.* **18** 41
[19] Emin D 1975 *Adv. Phys.* **24** 305
[20] Emin D 1993 *Phys. Rev.* B **48** 13691
[21] Alexandrov A S and Mott N F 1994 *Rep. Prog. Phys.* **57** 1197
[22] Alexandrov A S, Kabanov V V and Ray D K 1994 *Physica* C **224** 247
[23] Bryksin V V, Voloshin V S and Raitsev A V 1983 *Sov. Phys.—Solid State* **25** 820
[24] Alexandrov A S (ed) 2007 *Polarons in Advanced Materials* (Berlin: Springer)
[25] see e.g. Bi X X and Eklund P C 1993 *Phys. Rev. Lett.* **70** 2625
[26] Lakkis S, Schlenker C, Chakraverty B K, Bucher R and Marezio M 1976 *Phys. Rev.* B **14** 1429
[27] Schirmer O F and Salje E 1980 *J. Phys. C: Solid State Phys.* **13** L1067
[28] Moizhes B Y and Suprun S G 1984 *Sov. Phys.—Solid State* **26** 544
[29] Chauvet O, Emin D, Forro L, Aselage T L and Zuppiroli L 1996 *Phys. Rev.* B **53** 14450
[30] Koppitz J, Schirmer O F and Kuznetsov A I 1987 *Europhys. Lett.* **4** 1055
[31] Jermann F, Simon M, Böwer R, Krätzig E and Schirmer O F 1995 *Ferroelectrics* **165** 319
[32] Schirmer O F, Reyher H J and Wöhlecke M 1996 *Point Defects in Photorefractive Oxides* (*Insulating Materials for Optoelectronics*) ed F Agullo-Lopez (Singapore: World Scientific) p 93
[33] Briat B, Grachev V G, Malovichko G I, Schirmer O F and Wöhlecke M 2007 Defects in inorganic photorefractive materials and their investigations *Photorefractive Materials and Their Applications* vol 2, ed P Günter and J P Huignard (Berlin: Springer) p 9
[34] Merschjann C, Berben D, Imlau M and Wöhlecke M 2006 *Phys. Rev. Lett.* **96** 186404
[35] Bai Y S and Kachru R 1997 *Phys. Rev. Lett.* **78** 2944
[36] Hesselink L, Orlov S S, Liu A, Akella A, Lander D and Neurgaonkar R R 1998 *Science* **282** 1089
[37] Bogomolov V N, Kudinov E K, Mirlin D N and Firsov Yu A 1968 *Sov. Phys.—Solid State* **9** 1630
[38] Firsov Yu A 1969 *Sov. Phys.—Solid State* **10** 1537
[39] Beall F W 1968 *Color Centers in Solids* (New York: Academic University Press)
[40] Stoneham A M 1975 *Theory of Defects in Solids* (Oxford: Oxford University Press)
[41] Hayes W and Stoneham A M 1985 *Defects and Defect Processes in Nonmetallic Solids* (New York: Wiley)
[42] To J, Sokol A A, French S A, Katsoyannis N and Catlow C R A 2005 *J. Chem. Phys.* **122** 144704
[43] Stoneham A M, Gavartin J, Shluger A L, Kimmel A V, Muñoz-Ramo D, Rønnow H M, Aeppli G and Renner C 2007 *J. Phys.: Condens. Matter* **19** 255208
[44] Sicolo S, Palma G, DiValentin C and Pacchioni G 2007 *Phys. Rev.* B **76** 075121
[45] Lenjer S, Schirmer O F, Hesse H and Kool Th W 2002 *Phys. Rev.* B **66** 165106
[46] Kolodazhnyi T and Wimbusch S C 2006 *Phys. Rev. Lett.* **96** 249404
[47] Toyozawa Y 1961 *Prog. Theor. Phys.* **26** 29
[48] Emin D and Holstein T 1976 *Phys. Rev. Lett.* **36** 323
[49] Holstein T 1959 *Ann. Phys. NY* **8** 325
[50] Faust B, Müller H and Schirmer O F 1994 *Ferroelectrics* **153** 297
[51] Emin D 1982 *Phys. Today* **35** (6) 34
[52] Lax M 1952 *J. Chem. Phys.* **20** 1752
[53] Keil T 1965 *Phys. Rev.* **140** A601
[54] Wojtewicz A J, Kazmierczak M, Lempicki M M and Bartram R H 1989 *J. Opt. Soc. Am.* B **6** 1106
[55] Holstein T 1959 *Ann. Phys. NY* **8** 343
[56] Juppe S and Schirmer O F 1990 *Solid State Commun.* **76** 299
[57] Juppe S and Schirmer O F 1986 *Phys. Lett.* A **117** 150
[58] Rakitina L G, Zaritskii I M, Corradi G and Polgár K 1990 *Sov. Phys.—Solid State* **32** 654
[59] Emin D 1996 *Phys. Rev.* B **53** 1260
[60] Calvani P 2001 *Riv. Nuovo Cimento* **24** 1
[61] Shannon R D and Prewitt C T 1969 *Acta Crystallogr.* B **25** 925
[62] Lerner P, Legras C and Dumas J P 1968 *J. Cryst. Growth* **3** 231
[63] Bordui P F, Norwood R G, Bird C D and Calvert G D 1991 *J. Cryst. Growth* **113** 61
[64] Donnerberg H J, Tomlinson S M, Catlow C R A and Schirmer O F 1989 *Phys. Rev.* B **40** 11909
[65] Mehta A, Navrotsky A, Kumada N and Kinomura N J 1993 *Solid State Chem.* **102** 213
[66] Abrahams S C and Marsh P 1986 *Acta Crystallogr.* B **42** 61
[67] García-Cabañes A, Sanz-García J A, Cabrera J M, Agulló-López F, Zaldo C, Pareja R, Polgár K, Raksányi K and Földvári I 1988 *Phys. Rev.* B **37** 6085
[68] Bredikhin S, Scharner S, Klingler M, Kveder V, Redkin B and Weppner W J 2000 *Appl. Phys.* **88** 5687
[69] Falk M and Buse K 2005 *Appl. Phys.* B **81** 853
[70] Schirmer O F and von der Linde D 1978 *Appl. Phys. Lett.* **33** 35
[71] Müller H and Schirmer O F 1992 *Ferroelectrics* **125** 319
[72] Schmidt G, Albrecht M, Wippermann S, Blankenburg S, Rauls E, Fuchs F, Rödl C, Furthmüller J and Hermann A 2008 *Phys. Rev.* B **77** 035106
[73] Dutt D A, Feigl F J and DeLeo G G 1990 *J. Phys. Chem. Solids* **51** 407
[74] Nahm H H and Park C H 2008 *Phys. Rev.* B **78** 184108
[75] Koppitz J, Schirmer O F and Kuznetsov A I 1987 *Europhys. Lett.* **4** 1055

[76] Reyher H J, Schulz R and Thiemann O 1994 *Phys. Rev.* B **50** 3609
[77] Sweeney K L and Halliburton L E 1983 *Appl. Phys. Lett.* **43** 336
[78] Pape M, Reyher H J and Schirmer O F 2005 *J. Phys.: Condens. Matter* **17** 6835
[79] Gebhardt W and Kühnert H 1994 *Phys. Lett.* **11** 15
[80] Nagels P 1980 Experimental Hall effect data for a small polaron semiconductor *The Hall Effect and its Applications* ed C L Chien and C R Westlake (New York: Plenum) p 253
[81] Berglund C N and Braun H J 1967 *Phys. Rev.* **164** 790
[82] Herth P, Granzow T, Schaniel D, Woike Th, Imlau M and Krätzig E 2005 *Phys. Rev. Lett.* **95** 067404
[83] Corradi G, Meyer M, Kovacs L and Polgar K 2004 *Appl. Phys.* B **78** 607
[84] Chirila M M, Garces N Y, Halliburton L E, Evans D R, Route R K and Fejer M M 2003 *J. Appl. Phys.* **94** 301
[85] Kappers L A, Sweeney K L, Halliburton L E and Liaw J H W 1985 *Phys. Rev.* B **31** 6792
[86] Kitaeva G K, Kuznetsov K A, Morozova V F, Naumova I I, Penin A N, Shepelev A V, Viskovatich A V and Shigunov D M 2004 *Appl. Phys.* B **78** 759
[87] Merschjann C, Schoke B and Imlau M 2007 *Phys. Rev.* B **76** 085114
[88] Merschjann C, Schoke B, Conradi D, Imlau M, Corradi G and Polgar K 2009 *J. Phys.: Condens. Matter* **21** 015906
[89] Jermann F, Simon M, Böwer R, Krätzig E and Schirmer O F 1995 *Ferroelectrics* **165** 319
[90] Merschjann C, Berben D, Imlau M and Wöhlecke M 2006 *Phys. Rev. Lett.* **96** 186404
[91] Berben D, Buse K, Wevering S, Herth P, Imlau M and Woike Th 2000 *J. Appl. Phys.* **87** 1034
[92] Carnicero J, Carrascosa M, García G and Agulló-López F 2005 *Phys. Rev.* B **72** 245108
[93] Jhans H, Honig J M and Rao C N R 1986 *J. Phys. C: Solid State Phys.* **19** 3649
[94] Dhar A and Mansingh A 1990 *J. Appl. Phys.* **68** 5804
[95] Akhmadullin I S, Golenishev-Kutuzov V A and Migachev S A 1998 *Phys. Solid State* **40** 1012
[96] Arizmendi L, Cabrera J M and Agulló-López F 1984 *J. Phys. C: Solid State Phys.* **17** 515
[97] Hodgson E R and Agulló-López F 1987 *Solid State Commun.* **64** 965
[98] García-Cabañes A, Diéguez E, Cabrera J M and Agulló-López F 1989 *J. Phys.: Condens. Matter* **1** 6453
[99] Sugak D, Zhydachevskii Ya, Sugak Yu, Buryy O, Ubizskii S, Solskii I, Schrader M and Becker K D 2007 *J. Phys.: Condens. Matter* **19** 086211
[100] Zhang Y, Guilbert L and Bourson P 2004 *Appl. Phys.* B **78** 355
[101] Schirmer O F, Juppe S and Koppitz J 1987 *Cryst. Lattice Defects Amorphous Mater.* **16** 353
[102] Emin D 2003 *Models and Methods of High-T_c Superconductivity* vol 2, ed J K Srivastava and S M Rao (New York: Nova Science Publishers) chapter 11
[103] Merschjann C 2007 *PhD Thesis* University of Osnabrueck
[104] Gronenborn S, Sturman B, Falk M, Haertle D and Buse K 2008 *Phys. Rev. Lett.* **101** 116601
[105] Arizmendi L and Agulló-López F 1994 *Mater. Res. Bull.* (March) 33
[106] Haixian Xu, Donghwa Lee, Jun He, Sinnott S B, Gopalan V, Dierolf V and Phillpot S R 2008 *Phys. Rev.* B **78** 174103
[107] Chan H M, Zhuang Z and Smyth D M 1986 *Mater. Res. Soc. Symp. Proc.* **60** 95
[108] Bartram R H and Stoneham A M 1975 *Solid State Commun.* **17** 1593
[109] Parsons R, Cornish W D and Young L 1975 *Appl. Phys. Lett.* **27** 654